Université / UNIVERSITÉ de Cergy-Pontoise / Paris Seine

المدرسة الوطنية المتعددة التقنيات
Ecole Nationale Polytechnique

ECAM EPMI
GRADUATE SCHOOL OF ENGINEERING

École Doctorale Sciences et Ingénierie - ED n° 417

THÈSE DE DOCTORAT

Pour obtenir le grade de docteur délivré par

L'UNIVERSITÉ PARIS SEINE ET L'ÉCOLE NATIONALE POLYTECHNIQUE - COTUTELLE

Discipline : Génie électrique et électronique - Automatique

Présentée par

Islam ZIOUANI

Optimized Hierarchical Control for Distributed Generators in Smart MicroGrids

---

Directeurs de thèse: Prof. Abdelmoumen DARCHERIF et Prof. Djamel BOUKHETALA

Co-encadrante: Dr. Ikram ELABBASSI

Thèse présentée et soutenue à Cergy le 20 Janvier 2020 devant le jury composé de:

Mr. Abdelaziz HAMZAOUI	Professeur	IUT de Troyes	Rapporteur
Mr. Atallah BENALIA	Professeur	Université Amar Telidji Laghouat, Algerie	Rapporteur
Mr. Jean-Marc DEDULLE	Professeur	Grenoble INP	Examinateur
Mr. Rachid ILLOUL	MCF+HDR	Ecole Nationale Polytechnique, Algerie	Examinateur

Université / UNIVERSITÉ de Cergy-Pontoise / Paris Seine

المدرسة الوطنية المتعددة التقنيات
Ecole Nationale Polytechnique

ECAM EPMI
GRADUATE SCHOOL OF ENGINEERING

École Doctorale Sciences et Ingénierie - ED n° 417

THÈSE DE DOCTORAT

Pour obtenir le grade de docteur délivré par

L'UNIVERSITÉ PARIS SEINE ET L'ÉCOLE NATIONALE POLYTECHNIQUE - COTUTELLE

Discipline : Génie électrique et électronique - Automatique

Présentée par

Islam ZIOUANI

Optimized Hierarchical Control for Distributed Generators in Smart MicroGrids

---

Directeurs de thèse: Prof. Abdelmoumen DARCHERIF et Prof. Djamel BOUKHETALA

Co-encadrante: Dr. Ikram ELABBASSI

Thèse présentée et soutenue à Cergy le 20 Janvier 2020 devant le jury composé de:

Mr. Abdelaziz HAMZAOUI	Professeur	IUT de Troyes	Rapporteur
Mr. Atallah BENALIA	Professeur	Université Amar Telidji Laghouat, Algerie	Rapporteur
Mr. Jean-Marc DEDULLE	Professeur	Grenoble INP	Examinateur
Mr. Rachid ILLOUL	MCF+HDR	Ecole Nationale Polytechnique, Algerie	Examinateur

ملخص- يتعلق هذا العمل بتطوير نظام تحكم محسن لإدارة الطاقة الناتجة عن المولدات الموزعة غير المتجانسة ومصادر الطاقة المتجددة التي تشكل ميكرو شبكة ذكية. ميكرو شبكة هي نظام توزيع للطاقة يجمع بين مصادر الطاقة المتجددة والمولدات الموزعة ، فضلاً عن الأحمل الكهربي المحلية. يمكن أن تبادل الكهرباء مع شبكة الكهرباء ويمكن أن تعمل بشكل مستقل. الاستخدام الأمثل لميكرو شبكة هو توفير الطاقة للمناطق النائية أو المواقع غير القادرة على الوصول إلى الشبكة العامة. بالإضافة إلى ذلك ، تهتم شركات المرافق بدرجة أكبر باستخدام ميكرو شبكة لتوليد الطاقة بسبب متانتها وموثوقيتها وربحيتها. المولدات الموزعة مثل أجهزة تخزين الطاقة ومولدات الديزل هي مولدات يمكن التحكم فيها ويمكنها ضبط طاقة وفقًا لاحتياجات حمل كهربي ، في حين أن مصادر الطاقة المتجددة مثل توربينات الرياح والألواح الخلايا الكهروضوئية هي مولدات لا يمكن السيطرة عليها , وبتالي تستغل إلى أقصى طاقاتها. في هذا السياق، اقترحنا حلاً يستند إلى نهج هرمي يتكون من ثلاثة مستويات: داخلية ، أولية وثانوية. هذا الحل قادر على التحكم في المولدات الموزعة في ميكرو شبكة لتزويد المستهلكين المحليين دون أى انقطاع وتبادل الطاقة مع شبكة الكهرباء العامة مع الاستفادة القصوى من الطاقة المتجددة. المستوى الداخلي ينظم الجهد لكل مولد موزع ، بناءً على التحكم المتتالية ووحدة التحكم في الرنين النسبي. يولد التحكم الأساسي الجهد المرجعي للرقابة الداخلية التي يتمثل دورها الرئيسي في تنسيق المولدات الموزعة بطريقة لا مركزية من أجل تقاسم الطلب على الطاقة النشطة والطاقة التفاعلية بينهما. يعوض جهاز التحكم الثانوى عن انحراف الجهد عن القيم الساسية ومزامنة الجهد مع الشبكة الرئيسية للانتقال السلس.

كلمات مفتاحية- التحكم الهرمي ، العاكس الجهد ، ميكرو شبكة مرنة ، التحسين ، التحكم في تدلى الشامل

Résumé- Ce travail porte sur le développement d'un schéma de commande optimisé pour la gestion de la puissance générée par les générateurs distribués hétérogènes et les sources d'énergie renouvelable constituant un microrésau intelligent. Un microrésau est un système énergétique distribué associant des sources d'énergie renouvelables et des générateurs distribués, ainsi que des charges locales. Il peut échanger de l'électricité avec le réseau électrique et peut fonctionner de manière autonome. L'utilisation idéale d'un microrésau consiste à alimenter des régions ou des sites éloignés dans l'incapacité d'accéder au réseau public. En outre, les exploitants d'entreprises s'intéressent davantage à l'utilisation des microréseaux pour la production d'électricité, en raison de leur durabilité, de leur fiabilité et de leur rentabilité. Les générateurs distribués tels que les dispositifs de stockage d'énergie et les générateurs diesel sont des générations contrôlable qui peuvent ajuster leur puissance de sortie en fonction des besoins de la charge, tandis que les sources d'énergie renouvelable telles que les éoliennes et les panneaux photovoltaïques sont des générations non contrôlable qui exploitent leur puissance maximale. En ce sens, nous avons proposé une solution basée sur une approche hiérarchique composée de trois niveaux : interne, primaire et secondaire. Cette solution est capable de contrôler les générateurs distribués dans un microréseau pour alimenter les consommateurs locaux sans aucune interruption et pour échanger une puissance avec le réseau électrique tout en exploitant au maximum l'énergie renouvelables. La commande interne est responsable de la régulation de la tension de sortie de chaque générateur distribué, basée sur une commande en cascade et un contrôleur à résonance proportionnelle. La commande primaire génère la tension de référence de la commande interne dont le rôle principal est de coordonner les générateurs distribués de manière décentralisée afin de partager la demande de puissance active et de puissance réactive entre eux. La commande secondaire compense l'écart de tension par rapport aux valeurs nominales et synchronise la tension du microréseau avec le réseau principal pour une transition en douceur.
Mots clés : Commande hiérarchique, Onduleur de tension, microréseau flexible, Optimisation, Commande de statisme universel

Abstract-This work focuses on the development of an optimized control scheme for managing the power generated by heterogeneous distributed generators (DGs) and renewable energy sources (RESs) that constituting a smart microgrid. A microgrid is a distributed energy system that gathering a combination of renewable energy sources and distributed generators, as well as local loads. It can exchange power with the utility grid, and it can operate autonomously. The ideal use of a microgrid is to supply remote regions or locations that are unable to access the public grid. Moreover, utility operators become more interested in using microgrids for producing electricity due to their sustainability, reliability, and cost-effective. The DGs such as energy storage devices and diesel generators are dispatchable generations that can adjust their output power according to the load needs, whereas, the RESs such as wind turbines and photovoltaic panels are non-dispatchable generations which are used to exploit their maximum power. In this sense, we have proposed a solution based on the hierarchical approach that consists of three levels, inner, primary and secondary. This solution is able to control DGs in a hybrid microgrid for supplying continuously the local consumers without any interruption and for exchanging a smooth power with the utility grid while exploiting the maximum power from the renewables. The inner control is responsible to regulate the output voltage of each distributed generator which is based on cascaded control and Proportional-resonant controller. The primary control generates the reference voltage of the inner control which its principal role is to coordinate the distributed generators in a decentralized manner to share the active and the reactive power demand among them. The secondary control compensates the voltage deviation toward the nominal values as well as it synchronizes the microgrid voltage with the main grid for a smooth transition.
Keywords: Hierarchical Control, Flexible Microgrid, Universal droop controller, Voltage Source Inverters, Optimization

Acknowledgements

The work presented in this dissertation was carried out as part of a co-supervised thesis between Ecole Nationale Polytechnique (ENP) d'Alger, ECAM-EPMI (France), et Université de Paris Seine (France).

I would like to sincerely thank my supervisors, Professor Djamel Boukhetala and Professor Abdelmoumen Darcherif, for their outstanding professional advice and thoughtful comments making this work possible. Not only they provided me with technical guidelines, but they also taught me how to handle difficult situations.

I would like to thank Dr. Bilal Amghar et Dr. Ikram El Abbassi for their advice, dedication, and availability throughout this work.

I am very grateful to my family and friends for their sympathy and their presence during these four years.

I would also like to express my deepest sympathy to the colleagues from the two laboratories LCP of ENP and Quartz. As well as all the staff of the ENP and ECAM-EPMI.

Table of contents

List of figures

List of tables

Nomenclature

RES: Renewable energy source

DG: Distributed generator

PCC: Point of common coupling

MGCC: Microgrid central controller

VSI: Voltage source inverter

CSI: Current source inverter

AC: Alternative current

DC: Direct current

DER : Distributed Energy Resource

LV: Low voltage

MV: Medium Voltage

STS : Static transfer switch

SS: Static switch

PR: Proportional Resonance

CLTF: Closed loop transfer function

ESS: Energy storage system

THD: total harmonic distortion

Introduction

Motivated by climate change and global warming, most countries have adopted the Paris agreement in December 2015. This agreement draws lines to limit global warming and to exert efforts for reducing greenhouse gas emissions. According to the International Energy Agency, the largest source of greenhouse gas emissions comes from the electricity generation based on fossil fuels (i.e., coal, oil, natural gas, etc.). Hence, the world starts looking at alternative ways to generate electricity mainly in using clean and renewable sources such as wind energy, photovoltaic, thermal energy and tidal energy. These prime sources are distributed by nature and come with deferent form, some are DC sources, and others are AC sources.

In recent years, the concept of smart grids has gained more attention in the development of electrical grids due to high reliability, efficiency, and sustainability. Their physical distribution layer contains multiple renewable energy sources (RESs) and distributed generators as well as loads. The DGs such as energy storage devices and diesel generators are dispatchable generations which can adjust their output power according to the load needs, while, the RESs are non-dispatchable generations which are used to exploit their maximum power. However, high penetration of RESs into the distribution system can cause as many problems due to their intermittence and power variability. In this sense, the microgrid was introduced as a bridge, where the DGs operate in parallel with the RESs to cope with their intermittency and to smooth the exchanged power with the utility grid, this mode of operation is called the grid-connected mode. Moreover, the microgrid can operate in an islanded mode when it disconnects from the grid, in this case, the consumers are supplied locally.

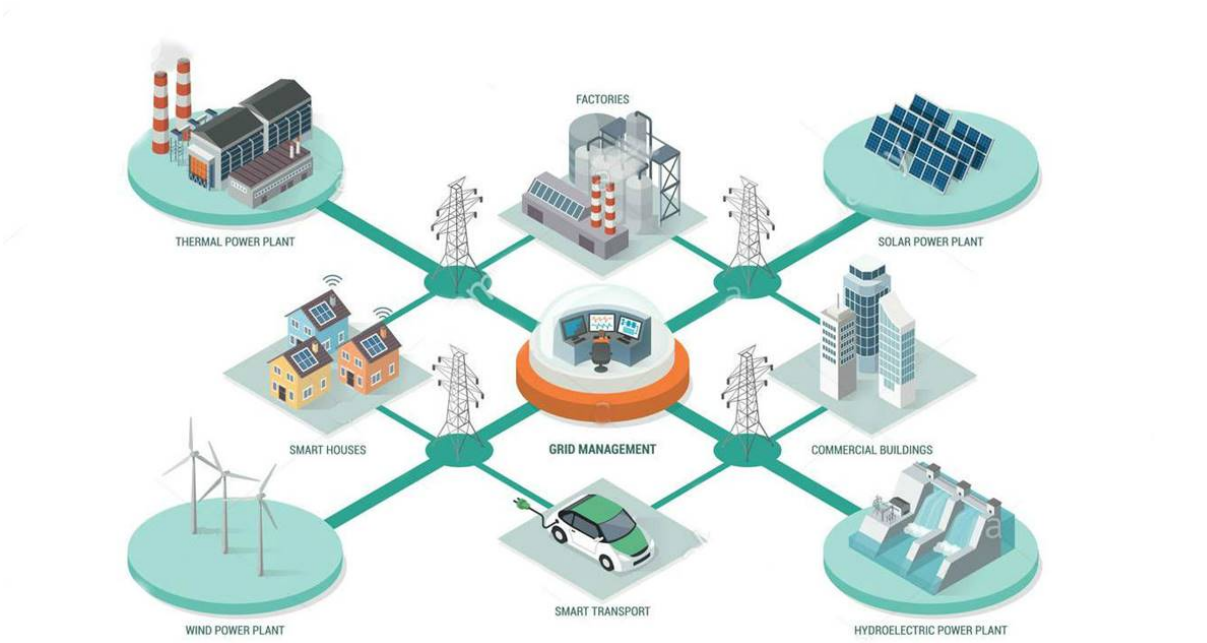

Fig. 1 Smart hybrid microgrid architecture

Thus, a microgrid effectively facilitates the integration of renewable sources at the physical distribution layer of smart grids which reduces emission and energy losses.

The DG or RES is interfaced with the microgrid via power electronic converter named inverter. This latter can act either as a current source or voltage source. The current source inverter (CSI) is appropriate for RES which transfers the maximum power to the local grid. On the other hand, the voltage source inverter (VSI) is appropriate for DG which regulates the voltage and frequency of the microgrid during the islanded mode.

Conventional, the inverter changes its controller according to the operation mode of the microgrid, in other words, the inverter behaves as a current source when the microgrid operates in grid-connected mode and as a voltage source when it operates in islanded mode or vice versa. Nowadays, VSI is the most topology adopted since it can change its behavior from a voltage source to the current source without changing the inner control strategy; it just needs to change the reference of the controller. This feature allows DGs to operate seamlessly either in grid-connected or in islanded mode.

The control strategy of the paralleled VSIs is based on the droop method which uses the local measurements to operate independently without external communications between the VSIs. This method was inspired by the conventional droop control of power system, where it is used by the synchronous generators to re-establish the active power balance. Furthermore, the objectives of the droop control in the microgrid are:

- Accurate active and reactive power sharing among the paralleled VSIs in proportion to their power ratings.
- Stabilize the microgrid voltage amplitude and frequency at the microgrid common bus (or point common coupling PCC).
- Inject the demanded power when the microgrid is operated in grid-connected mode.

In order to achieve these objectives, several droop methods were proposed in the literature. Recently, a new method is developed by Q.-C. Zhong *et al.* [102]. which called the universal droop control. This method can operate in an islanded mode which is robust to disturbances, noise and component mismatches. Moreover, it works regardless of the output impedance of the inverters.

However, the universal droop control can't handle the grid-connected mode, and it would cause a deviation in amplitude and frequency of the islanded microgrid voltage which leads to phase difference with the utility grid. In this sense, we have ameliorated the universal droop control, and we have enhanced it via a hierarchical structure which becomes its primary control. The secondary control of the hierarchical structure is used to compensate for the voltage and frequency deviation caused by the primary control and synchronizes the microgrid voltage with the grid voltage in order to ensure a smooth transition. The secondary control can be classified into two structures

- A centralized structure is implemented in the microgrid central controller (MGCC) which is suitable for islanded operation.
- A Decentralized structure allows DG units to interact with each other which is suitable for grid-connected operation.

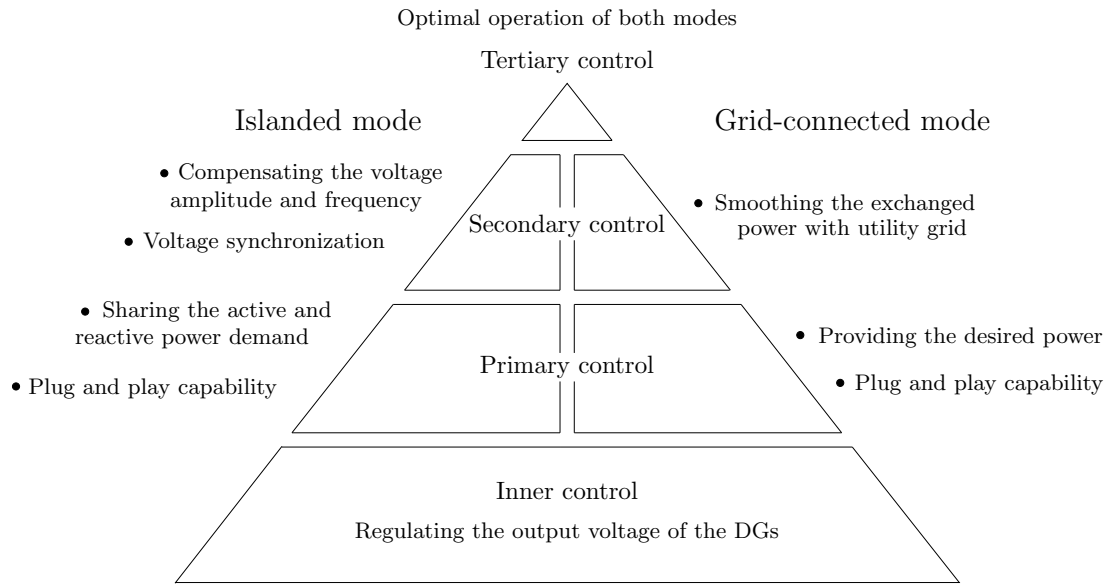

Fig. 2 The levels of Hierarchical Control of a Microgrid

The centralized structure is adopted throughout the thesis. The proposed hierarchical control allows a microgrid to operate either in islanded or in a grid-connected mode with a smooth transition between them. In the islanded mode, the microgrid is disconnected from the main grid where operates autonomously, while the objectives are to achieve an accurate power sharing among the paralleled DGs in proportion to their power ratings, regardless of their output impedance, as well as maintaining a close regulation of the voltage amplitude and frequency at the PCC. For a seamless connection to the grid, the voltage at PCC must be synchronized to the voltage of the grid using a synchronization loop that reduces the phase angle between them. In grid-connected mode, the DGs are controlled in order to generate the desired power that scheduled by a smart supervisor located in the Microgrid central controller (MGCC). The supervisor is the tertiary level of the hierarchical control which deals with the energy management of the local sources and exchanged energy with the utility grid, this level is not considered in my thesis.

Based on previous work on the control of distributed generators and microgrids, this thesis is structured as follows:

Chapter 1 introduces the different definitions of microgrids with a detailed study of operating modes and the different control levels of a microgrid, followed by the thesis objectives.

Chapter 2 presents the adopted solver of the optimized problem for finding optimal parameters of the hierarchical control. The solver is based on a metaheuristic algorithm called self-learning particle swarm optimizer (SLPSO) which is an improved variation of particle swarm optimization (PSO) .

Chapter 3 presents a cascaded control loop (voltage and current) of the distributed generator where the voltage source inverter is modeled and a virtual impedance is proposed to improve the power quality.

Chapter 4 describes some of the droop techniques used to control distributed generators connected in parallel in a microgrid and proposes an improved universal droop control method to deal with the weaknesses of conventional droop control. Moreover, the secondary control for voltage restoration and the synchronization process is presented, as well as an optimal controller design technique is given.

Chapter 1

State of the Art

1.1 Introduction

In recent years, there has been growing interest in integrating Distributed Energy Resources (DERs) into small-scale grids, in order to cope with the increasing demand and to confront global warming. DER components include a wide range of power technologies, such as photovoltaic panels, fuel cells, wind-turbines, micro-turbines, and storage systems [42].

Renewable energy sources (RESs) have gained rapid development, which makes them affordable. They are clean for the environment and inexhaustible. These advantages promote the security of energy by reducing the use of fossil fuel and allow for supporting the utility grid in remote sites and rural areas [70].

However, high penetration of RESs into the distribution layer of the utility grid can cause as many problems such as power flows, voltage drops, and voltage fluctuations, due to their intermittency and power variability [81].

In order to fix these problems and overcome these challenges, a new paradigm has been proposed and is called the Microgrid. A Microgrid can be conceived as a small-scale power grid, that consists of multi-type of generation units (dispatchable and non-dispatchable), storage systems and controllable and critical loads, with the ability to operate autonomously without connecting to the utility grid [39].

The concept of Microgrid promotes decentralized and coordinated control, in which the deferent type of power generation systems (RESs, energy storage systems, dispatchable generations,etc.) can operate in parallel and cooperate in a decentralized and distributed manner. Thus, it generates electrical power locally and improves power quality [50].

Previously, and before the Microgrid concept appeared, many researchers were interested in integrating the distributed generations (DGs) based on RESs. The scientific community realized that the unclear definition of DG based on RES would lead to interference and fuzziness, which making research more difficult.

The stochasticity on the power generated from renewable energy sources would cause large disturbances in the utility grid, where it complicates the control, and eventually leads to an unstable system and may result in a blackout. From this perspective, Microgrids will permit the large-scale penetration of intermittent renewables into the distribution layer of the utility grid while maintaining stability.

Moreover, the improved development in energy storage systems and power electronic devices, have permitted microgrids to become a feasible solution. Hence, a microgrid is a key element to integrate distributed energy resources, renewables as well as energy storage systems. Many researchers claim that the future grid will be seen as an interconnected microgrid cluster [79].

1.2 Definition of microgrid

Microgrids cannot be presented as a new concept since small-scale power grids have long existed in remote areas, where interconnection with the main grid is not possible for technical or economic reasons [75]. Nowadays, the concept and definition of microgrids have changed to provide customers with sustainable energy choices in terms of renewable energy integration, network reliability, flexibility, and economy [97].

Microgrids have the potential to maximize the overall efficiency of the system, power quality, and allow customers to control their electricity supply [71]. A microgrid is defined as an energy system incorporating intelligent management and consists of a variety of components, including [84]: distributed energy resources (DER) (photovoltaic, small wind tur-

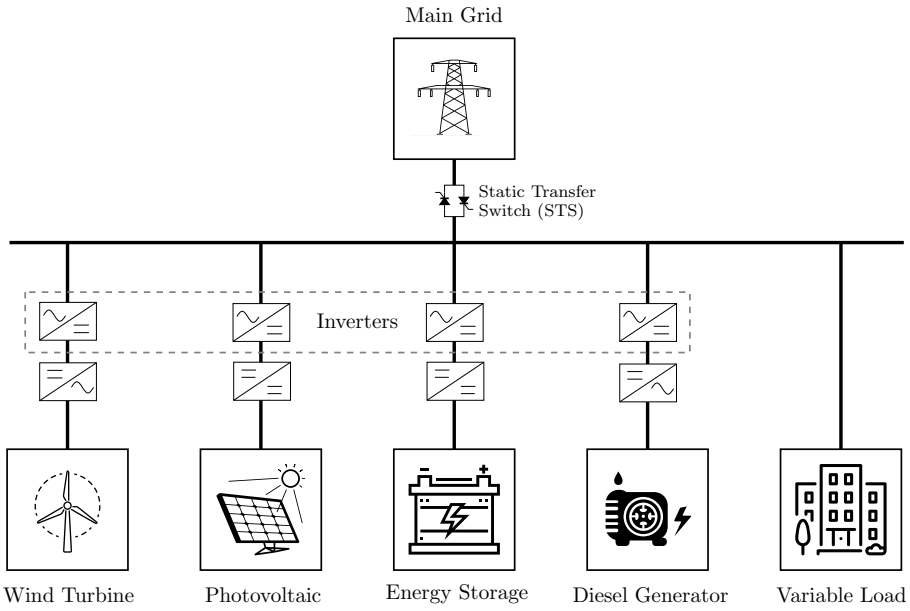

Fig. 1.1 Microgrid architecture.

bines, fuel cells, combustion engines, micro-turbines, etc.); Distributed energy storage devices (DES) (flywheels, superconducting inductors, batteries, etc.), they can be used to absorb excess power and discharge to cover the power deficit, thus, they help to improve the reliability; controllable loads usually located nearby and may include a single/multiple clients or a group of charges (hospital, school or campus, military base). The characteristics and dynamics of each microgrid component present a major challenge in controlling and operating with the power grid [76]. In the near future, microgrid technology will improve the security of a mini-grid or macro-grid at a local or even regional level by helping to support the network during major failures. Figure 1.1 shows the structure of a Low Voltage (LV) microgrid that connects to the Medium Voltage (MV) network through a transformer, consisting of four DER systems. The DGs are wind turbine, photovoltaics, energy storage system and diesel generator. The microgrid is connected to the main grid often through a static transfer switch (STS) at the point of common coupling (PCC). When the microgrid is operating in grid-connected mode, both the DGs and the main grid provide power to the loads. In the event of a power failure, the STS opens to isolate the microgrid from the main grid. Transferring the microgrid from grid-connected mode to islanded mode which allows the microgrid to con-

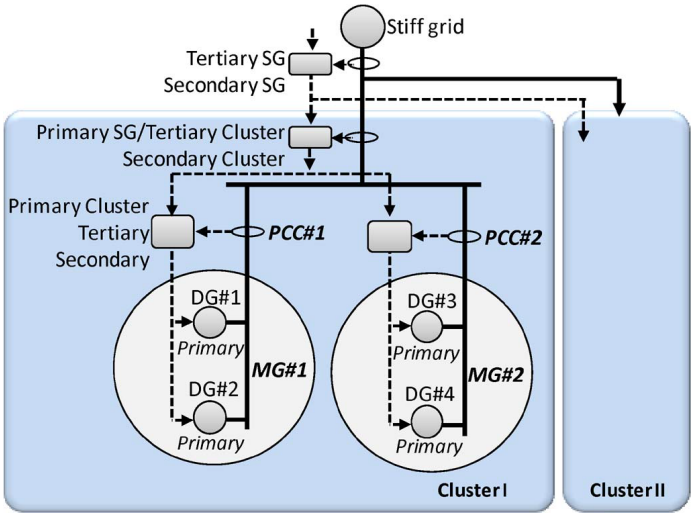

Fig. 1.2 Interconnected Microgrids [29].

trol the load voltage and provide uninterrupted power to all its critical loads. When the fault is cleared, the microgrid must be resynchronized with the main grid before closing the STS to return the system to the grid-connected mode [86]. If a slight voltage imbalance occurs or the local loads are not sensitive to imbalances, the microgrid can remain connected [24].

As shown in Figure 1.1, there are three types of power generation resources: conventional rotary generators (hydroelectric), units interfaced by power electronics (photovoltaic system), and power electronics interfaced with storage units (wind turbine with storage battery). A production unit may have a controlled output (dispatchable) or an uncontrollable output (non-dispatchable).

The objective of a microgrid is to mitigate the environmental impacts of traditional power systems, improve their performance and better unit commitment. Microgrids enter the vision of the smart grid by providing a solution in which an intelligent network is gradually implemented through multiple microgrids that interact with each other. Figure 1.2 shows an illustration of the pictorial diagram of how microgrids enter the vision of the smart grid.

1.3 Operating modes of microgrid

The operation of the microgrid can depend on the conflicting interests between the different actors involved in the power supplying, such as the operators of the power grid, the owners

of the distributed generators, the energy suppliers, etc., as well as the customers. The optimal operation of the microgrid is based on economic, technical or environmental aspects. Four modes of operation have been identified by the IEEE Std 1547 [9], namely: the grid-connected mode, the transition mode, the islanded mode, and the reconnection mode.

1.3.1 Grid-connected mode

The microgrid is connected to the main grid according to its energy needs, it can partially or totally receive the energy or send the excess of its electrical energy to the main grid when its total output of DGs exceeds the consumption.

1.3.2 Transition to islanded mode

It is recommended that the DGs be available to support the microgrid voltage and frequency for a period of time while the interconnection and protection devices take over to make a successful transition.

1.3.3 Islanded mode

When the main grid encounters a problem, where there are actions planned (for example, to perform maintenance operations), the microgrid can easily disconnect from the main grid and remain operational and functional as a stand-alone entity for supply the local loads. In this mode, the DGs must have a sufficient reserve margin which is in the function of the load factor, the load amplitude, the type of the load, the load reliability requirements, and the availability of the DG. To balance the load and the generation in the autonomous mode, several techniques are suggested in the literature such as load-following, load-management and load shedding [48]. In addition, it is emphasized that transient stability should be maintained for load variations, a failed DG unit, and autonomic faults. It is also suggested that the adaptive relay can be implemented to provide adequate protection for a variety of operating modes of the system.

1.3.4 Reconnecting mode

To reconnect the islanded microgrid to the main grid, the monitoring shall indicate that the appropriate conditions exist to synchronize the system. It is recommended that after a disturbance in the main grid, no reconnection should take place until its voltage is within the tolerable range. In addition, the phase voltage and the frequency between the two systems should be within acceptable limits as specified in IEEE Std 1547 in order to initiate a reconnection [9].

1.4 Hierarchical Control in Microgrid

Power generation within a microgrid are heterogeneous, where some sources generate DC power, and others generate variable frequency AC power. Since the type of microgrid considered in this thesis is a synchronous AC grid, thus, the distributed generations are interfaced with it via power electronic inverters. Therefore, proper control of these inverters is a prerequisite in order to ensure a stable and economically efficient operation of a microgrid. The principal duties of a control scheme in a microgrid are:

- voltage amplitude and frequency regulation for both operating modes
- Maintaining power balance and load sharing during islanded mode
- Microgrid synchronization and resynchronization with the main grid,
- Optimal Power flow between the microgrid and the main grid in grid-conned mode,

In literature, there are many control strategies that can be classified as centralized, decentralized and distributed control which have been proposed to address the stated challenges. They have later been collected into a hierarchical control scheme due to the different significances and time scales of the microgrid system. The Hierarchical control strategy consists of four levels, namely the inner, primary, secondary, and tertiary controls.

1. *Inner Control (Level 0)*: This level controls and regulates the output voltage and current of the VSI.

2. *Primary Control (Level 1)*: It is a local controller that provides a proportional power sharing among the DGs and mitigates the circulating current that appears when VSIs operate in parallel. The idea comes from the traditional primary control of the synchronous generator that realized by turbine-governors and voltage regulator.

3. *Secondary Control (Level 2)*: When power-sharing is achieved by the primary control, the frequency and the voltage amplitude may deviate from their nominal values. Thus, the secondary control is needed to restore the microgrid voltage; this controller is centralized and located in MGCC where it sends the corrected values by using low bandwidth communications to all paralleled VSIs. MGCC can also contain a synchronization loop to facilitate the transition from island to grid-connected mode.

4. *Tertiary Control (Level 3)*: This is the last and the slowest control level that is responsible to schedule the power of each DGs. It depends on global economic and current energy prices. One of its objectives is to achieve the optimal operation during islanded mode and optimal power flow during the grid-connected mode.

1.5 Thesis Objectives

The purpose of this thesis is to develop an optimized control scheme for distributed generators in a hybrid microgrid that fulfills all the following requirements:

Operating in autonomous mode (Islanded mode):

- Maintain the microgrid stability in islanded mode (where the main grid is not presented).
- Provide a high power quality to the local consumer.
- Support the plug and play (each generator can connect, disconnect or reconnect at any moment).
- Exploit the maximum power from renewable sources.

Operating in grid-connected mode:

- Import/Export a smooth power from the main grid.
- Respecting the grid code when the microgrid exports its surplus power.
- Support the plug and play
- Exploit the maximum power from renewable sources.

Transition mode:

- Ensuring the stability when the microgrid is attempting to connect/disconnect to/from the main grid.

1.6 Conclusion

This chapter summarizes the definition and control structure of the microgrid and its deferent operating modes. Hierarchical control has been described showing the different levels of control (inner, primary, secondary and tertiary) and the thesis objectives have been given. The zero level is the inner control which is dealing with the regulation of the output voltage of VSI, where it is based on cascaded proportional-resonant controllers. The first level is the primary control which is used to share the active and reactive power among the paralleled VSIs by sacrificing the amplitude and the frequency of the microgrid voltage at PCC. Therefore, the second level which is the secondary control comes to compensate the deviations in the amplitude and the frequency caused the primary control as well as to ensure a seamless transition from islanded mode to grid-connected mode.

Chapter 2

Optimization SLPSO

2.1 Introduction

The objective of optimization is to find the best solution to a constrained problem. Recent years, many researchers have proposed different techniques to solve linear and non-linear optimization problems. An optimization problem is modeled as a cost function describing the problem, under a set of constraints restricting the solution space for the problem.

Nonetheless, most conventional methods of optimization concentrate on evaluating the first derivatives to locate the optima on a restricted surface. Due to the difficulties in evaluating the first derivatives, recently, many derivative free optimization algorithms have emerged to find the optimum for many rough and discontinuous optimization problems.

Nowadays, the problem of optimization is represented as an intelligent search problem, where at least one agents are used to decide the optimum in a search space, representing the restricted surface for the problem of optimization. Inspired by the biological species' natural adaptations, Holland echoed Darwinian theory through his most popular and well-known genetic algorithm (GA) [40]. Figure 2.1 shows the rough classification of optimization algorithms.

In mid 1990s, Eberhart and Kennedy proposed an alternative solution to the complex non-linear optimization problem by imitating the behavior of bird flocks which called particle swarm optimization (PSO) [49]. By integrating regional exchange of information through

the nearest modification of velocity, prematurely the flock or swarm converged uniformly. Therefore, a random disturbance or craziness was introduced in the particle velocities resulting in sufficient variation and subsequent life-like swarm dynamics.

Such parameters were eventually omitted as the flock seemed to converge as well without them on attractors. Though PSO is an effective tool for global optimization problems, it is weak though solving complex problems or dynamic problems. This is especially true for the original PSO algorithm.

To improve PSO performance to solve complex problems, Changhe Li presented a novel algorithm, called self-learning PSO (SLPSO) [52]. In SLPSO, each particle has four different learning strategies in the search space. The coordination of the four training methods is applied independently through an evolutionary process, Which can allow that particle to choose an optimal training strategy based on its own local fitness landscape properties. This flexible training method allows to automatically balance the behavior of exploration and exploitation for each particle in the entire search space during the whole running process.

2.2 Classical PSO

PSO is a multi-agent parallel search technique which a swarm of particles move through the search space. In the search space, the particle keeps track of its coordinates that are correlated with the best solution it has achieved so far. This value is named pbest, the best value obtained so far by any particle in the particle's neighbors is another best value recorded by a particle. This is called the lbest location. If a particle takes the entire population as its topological neighbors, the highest value is a global best and is called gbest. The concept of PSO consists of changing the speed of each particle (accelerating) to its pbest and lbest positions at each time step. Acceleration is a random term weighs, generating separate random numbers for acceleration to pbest and lbest locations.

PSO was introduced in 1995 for the first time. It is a very efficient stochastic tool for optimization problems. Recently, this promising research area has attracted more and more researchers. It is shown that PSO has a quicker, cheaper way of achieving better results compared to other approaches. Another reason PSO is attractive is that few parameters need to

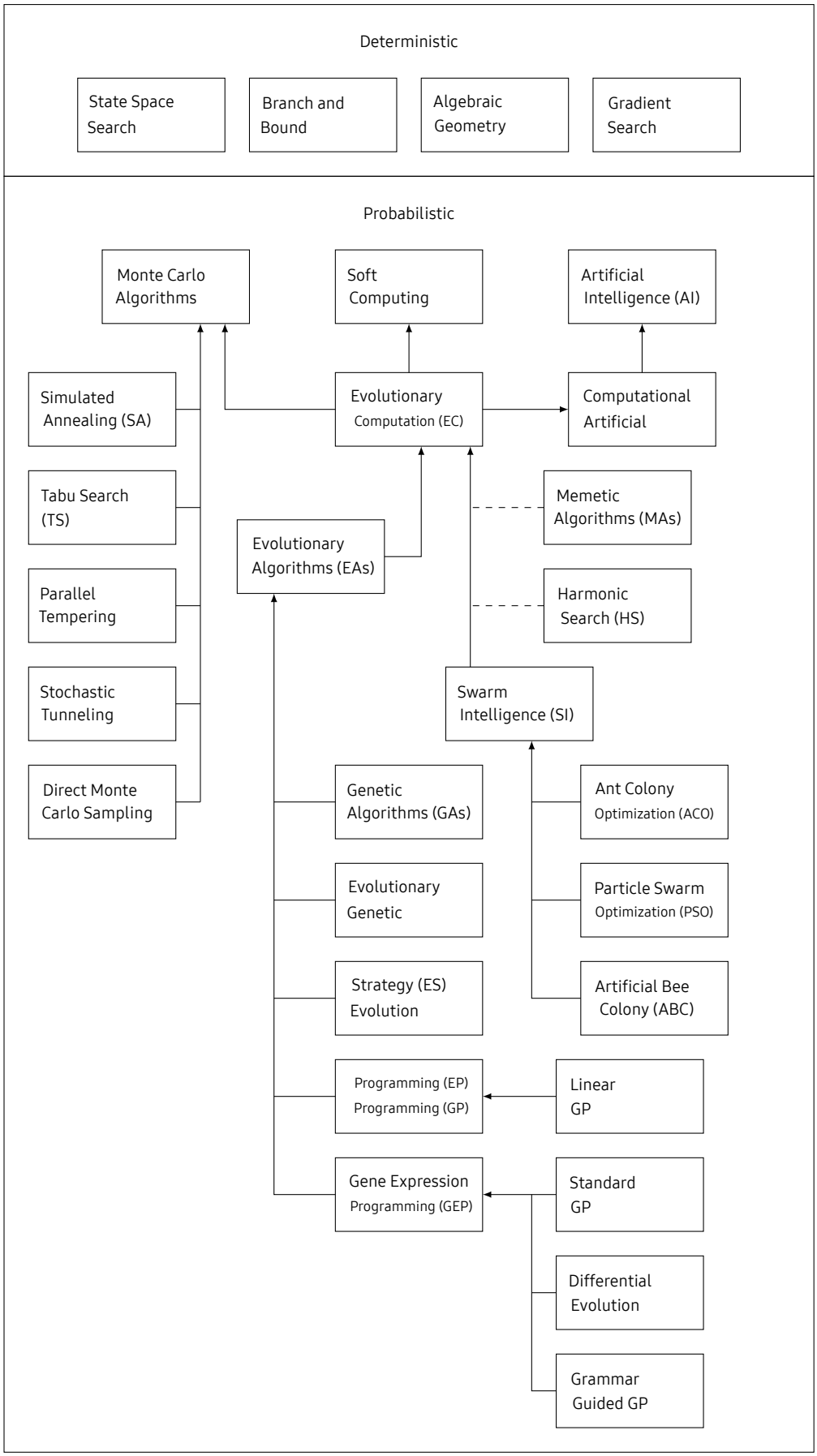

Fig. 2.1 Classification of global optimization algorithms. [95].

be adjusted. One version works well in a wide variety of applications, with slight variations. PSO has been used for methods that can be used across a wide range of applications, as well as for particular focused applications.

In search space of dimension D, particle k of swarm S is represented by position vector $x_k = (x_k^1,\ x_k^2,\ \ldots,\ x_k^D)$ and velocity vector $v_k = (v_k^1,\ v_k^2,\ \ldots,\ v_k^D)$. The quality of its position is determined by the value of the objective function at this point. This particle keeps in memory the best position by which it has already passed, that is noted $pbest_k = \left(pbest_k^1,\ pbest_k^2,\ \ldots,\ pbest_k^D\right)$ (best position) The best position reached by the particles of the swarm is noted $gbest = \left(gbest^1,\ gbest^2,\ \ldots,\ gbest^D\right)$ (best global position). At the start of the algorithm, the particles of the swarm are randomly initialized in the search space of the problem. Then, at each iteration, each particle moves, linearly combining the three components mentioned above. Indeed, at iteration $t+1$ the velocity vector and the position vector are calculated from the equation (2.1) and (2.2), respectively:

$$v_k^d(t+1) = \omega v_k^d(t) + c_1 \cdot r_k^d \cdot \left(pbest_k^d - x_k^d(t)\right) + c_2 \cdot r_k^d \cdot \left(gbest^d - x_k^d(t)\right) \tag{2.1}$$

$$x_k^d(t+1) = x_k^d(t) + v_k^d(t+1) \tag{2.2}$$

Where ω is constant, called coefficient of inertia; c_1 et c_2 are two constants, called acceleration coefficients; r_1 et r_2 are two random numbers uniformly in $[0,1]$, at each iteration t and for each dimension. The three components mentioned above (i.e. of inertia, cognitive and social) are represented in the equation (2.1) by the following terms:

1. $\omega v_k^d(t)$: corresponds to the component of inertia of displacement, where the parameter ω controls the influence of the direction of movement on the future displacement, $\omega \in \begin{bmatrix} 0.4 & 1.4 \end{bmatrix}$
2. $c_1 \cdot r_k^d \cdot \left(pbest_k^d - x_k^d(t)\right)$: corresponds to the cognitive component of the displacement, where the parameter c_1 controls the cognitive behavior of the particle, $c_1 \in \begin{bmatrix} 1.5 & 2 \end{bmatrix}$
3. $c_2 \cdot r_k^d \cdot \left(gbest^d - x_k^d(t)\right)$: corresponds to the social component of displacement, where the parameter c_2 controls the social fitness of the particle, $c_2 \in \begin{bmatrix} 2 & 2.5 \end{bmatrix}$

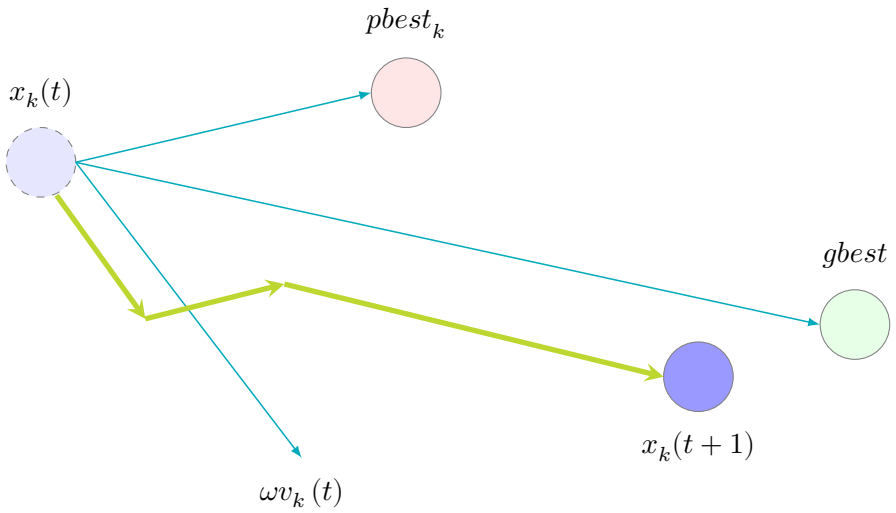

Fig. 2.2 Displacement of a particle.

Algorithm 1 Particle Swarm Optimization

```
for Each particle x_k do
    Initialize x_k randomly in the search space and v_k = 0
end for
while the stopping criterion is not satisfied do
    for Each particle x_k do
        Calculate the value of the objective function f(x_k)
        if f(x_k) is better than f(pbest_k) then
            Update pbest_k = x_k
        end if
        if f(pbest_k) is better than f(gbest) then
            Update gbest = pbest_k
        end if
        Calculate the particle speed v_k according to (2.1)
        Move the particle x_k according to (2.2)
    end for
end while
```

The original PSO algorithm framework is shown in Algorithm 1. Figure 2.2 shows the displacement of a particle. In PSO, each particle shares with its neighbors the information. The second and third components on the right of equation 2.1 are respectively referred to in PSO as cognition and social components. The updating formula equations show that PSO blends each particle's intelligence component with a group's social particle portion. The social component implies that individuals disregard their own experience and change their actions in the group's neighborhood according to the previous best particle. On the other

hand, the component of cognition treats individuals as isolated beings and only adapts their behavior to their own experience.

2.3 Improvements of PSO

Numerous enhancements have been proposed for the Particle Swarm Optimizer.

2.3.1 Inertia weight

Some of the earliest changes to the original PSO were intended to further improve the convergence rate of the algorithm. One of the most commonly used improvements is Shi and Eberhart's introduction of inertia weight [87]. The weight of inertia is a scaling factor associated with the velocity during the previous step, resulting in a new equation of velocity updates.

$$v_{i,j}(t+1) = \omega v_{i,j}(t) + c_1 r_{1,j}(t)\left[y_{i,j}(t) - x_{i,j}(t)\right] + c_2 r_{2,j}(t)\left[\hat{y}_j(t) - x_{i,j}(t)\right] \tag{2.3}$$

By setting the original PSO velocity update equation $\omega = 1$. Shi and Eberhart investigated the impact ofω values in the range $[0, 1.4]$, as well as varying ω over time [87]. Their results show that choosing $\omega \in [0.8, 1.2]$ results in faster convergence, but that larger ω values (> 1.2) this leads to more failures to converge.

The inertia weight governs how much of the previous velocity should be retained from the previous time step. To briefly illustrate the effect of ω, let $c_1 = c_2 = 0$. Now, a ω value greater than 1.0 will cause the particle to accelerate up to the maximum velocity v_{max} (or $-v_{max}$), where it will remain, assuming the initial velocity was non-zero. A ω value less than 1.0 will cause the particle to slowly decelerate until its velocity reaches zero. When $c_1, c_2 \neq 0$, the behavior of the algorithm is harder to predict, but based on the results of Shi and Eberhart [87] it would appear that ω values close to 1.0 are preferable.

Another series of experiments were carried out to explore the relationship between v_{max} and the inertia weight [88]. In this experiment, for the single function studied, it was found

that an inertia weight of 0.8 produced good results, even when v_{max} = x_{max}. Nevertheless, the best performance was again obtained by using a weight of inertia that decreased 0.9 to 0.4 during the first 1500 iterations. During a simulation, more experimental tests were conducted with an inertia weight set to decrease linearly from $0.9$to 0.4, this time using four separate objective functions [89].

This configuration allows the PSO to explore a large area at the start of the simulation run (when the inertia weight is high) and to refine the search later using a lower inertia weight. The weight of the inertia can be compared with the temperature parameter found in Simulated Annealing [51]. The Simulated Annealing algorithm has a process called the temperature schedule which is used to reduce the system temperature gradually. The higher the temperature, the higher the likelihood that the algorithm will explore a region outside the current local minimum attraction basin. Thus an adaptive inertia weight in the Simulated Annealing algorithm can be seen as the equivalent of a temperature schedule.

2.3.2 Fuzzy Inertia Weight

Shi and Eberhart have recently suggested a technique for dynamically changing the inertia weight using a fuzzy controller [99]. A fuzzy controller is a system that can be used to convert a linguistic description of an issue into a model that can be used to predict a numerical variable, provided numerical inputs. [21]. In other words, if a person can explain approximately how a parameter should be modified when analyzing the data, the fuzzy controller can capture that information. Some knowledge of the impact of inertia weight has been accrued over the many experimental studies conducted, making a good option for a blurred weight regulator. Shi and Eberhart's proposed controller uses the existing inertia weight and the feature value corresponding to the best solution found to date, $f(\hat{y})$. Since most problems have different scales of function values, the value of $f(\hat{y})$ must be normalized. Equation 2.4 Presents a possible scaling technique for the function values:

$$f_{norm}(\hat{y}) = \frac{f(\hat{y}) - f_{min}}{f_{max} - f_{min}} \tag{2.4}$$

The values f_{max} and f_{min} are based on the issue and must be understood beforehand or some calculation must be available. Shi and Eberhart have opted to use three fuzzy membership functions, corresponding to three fuzzy sets (low, moderate, high) that can be used by the input variables. The fuzzy controller's output is the suggested improvement in the inertia weight quality. Some fine-tuning is necessary to specify the essential values for the fuzzy membership functions, but that is the point of first using a fuzzy controller: these parameters are known approximately from previous experience.

The fuzzy adaptive inertia weight PSO was compared to a PSO using a linearly decreasing inertia weight. The results indicated that for certain parameter settings, the fuzzy inertia weight PSO showed improved performance on some of the functions tested. Ironically, the blurred inertia weight approach had a greater advantage over the unimodal form in the test suite. This behavior is easily explained: unimodal functions do not have a local minimum, so at every iteration an optimal inertia weight can be calculated. Logically, a large inertia weight at the beginning of the run will allow the PSO to locate the approximate region where the minimizer is located faster.

After entering this location, the inertia weight should be gradually reduced to slow the particle motion, allowing smaller features to be placed on the surface of the object. This method can be approximated by linearly reducing the weight of inertia over time, but this mechanism does not ' know ' whether the PSO has found the area where a smaller weight of inertia should be used. Sometimes it may take the PSO longer to reach this field, sometimes it quickly finds it. The adaptive fuzzy controller can predict which type of behavior is more acceptable. The rules in the fuzzy controller effectively reduce the weight of the inertia at a level proportional to how near the PSO is to the minimum, determined by how close $f_{norm}\,(\hat{y})$ is to zero. Nonetheless, it is more difficult to find an optimal inertia weight when dealing with a function that contains multiple local minimals. If a particle has already ' stumbled on ' the basin containing the global minimum, the weight of inertia can be significantly reduced to allow the PSO to conduct a fine-grained search in that basin. On the other side, if the swarm has only found a good local minimum nearby, The correct inertia weight setting would be a slightly higher value to enable the PSO to escape the local minimum attraction basin. The

adaptive weight regulator can't tell the difference between being stuck in a better one (i.e. small value for $f_{norm}(\hat{y})$ local minimum, and near to the average unimodal feature.

The adaptive fuzzy weight controller is a promising strategy for maximizing the weight of inertia, but difficulties in implementing it, such as understanding the values of f_{max} and f_{min}, makes it difficult to implement in a generic way.

2.3.3 Constriction Factor

Recently, work by Clerc [18] specified that a restriction factor can contribute to convergence. Among other things, the constriction factor model describes a way to choose the values of ω, c_1 and c_2 so that convergence is ensured. By picking these values appropriately, the values need to be clamped of $v_{i,j}$ to the range $[-v_{max}, v_{max}]$ is obviated.

A revised equation of velocity updates corresponding to one of several models of constraints, is presented in equation 2.5:

$$v_{i,j}(t+1) = \chi\left(v_{i,j}(t) + c_1 r_{1,j}(t)\left(y_{i,j}(t) - x_{i,j}(t)\right) + c_2 r_{2,j}(t)\left(\hat{y}_j(t) - x_{i,j}(t)\right)\right) \tag{2.5}$$

Where:

$$\chi = \frac{2}{\left|2 - \varphi - \sqrt{\varphi^2 - 4\varphi}\right|} \tag{2.6}$$

and$\varphi = c_1 + c_2, \varphi > 4$

Eberhart and Shi compared the output of a swarm using the clamping $vmax$ to one using the restriction factor only. Their results showed that using the constriction factor (without clamping the speed) typically resulted in a higher convergence rate. However, on some of the test functions, the PSO with the restriction factor failed to reach the specified error threshold within the allocated number of iterations for this problem. According to Eberhart and Shi, the issue is that the particles are too far away from the target search area. In order to mitigate this effect, they also decided to apply clamping to the implementation of the restriction variable, setting the parameter $vmax$ equal to $xmax$, the search space size.

2.4 Self-learning Particle Swarm Optimizer

So far, for all particles, most PSO algorithms globally use a single learning pattern, meaning that all particles in a swarm use the same learning strategy, which makes it unable to tackle multiple complex situations. Actually, because of different fitness environments challenges, it needs to create an intelligent system with different characteristics rather than a common training pattern to cope with various complex situations.

This section will present a novel algorithm called self-learning PSO (SLPSO) to add more knowledge to the individual particle. It will define the SLPSO working mechanism systematically in the following aspects. First, a set of four learning strategies are introduced that have different properties to help particles deal with different properties of fitness landscapes. Secondly, an adaptive learning system is introduced to enable each particle to adapt the best learning strategy to its local fitness landscape. Third, an information update method for the best global particle is defined in order to extract useful information from improved particles. Fourthly, a monitoring system is developed that can accurately determine whether or not a general particle has converged. Fifthly, to increase diversity, a restart scheme is introduced to create new swarms composed of rebooted particles separated from old swarms. Finally, for general problems, a generalized parameter tuning approach is implemented.

In addition, multiple population methods are used to encourage particles in the fitness landscape to explore unseen areas. How to organize these components systematically and make them work efficiently.

2.4.1 Learning Strategies in SLPSO

Inspired by the concept of labor division, could assign different roles to particles, e.g., converging to the global best particle, exploitation of its personal best position, exploring new promising areas, or jumping out of local optima. Which role a particular particle should play is determined by the local fitness landscape where it is. To assign to a particular particle individual level of intelligence, need to consider the possible situations of the local fitness landscape.

Defines four learning techniques and associated learning operators used in SLPSO on the basis of the above concept. In SLPSO, for each particle, the learning information comes from four sources: the gbest particle archive (abest), its individual pbest position, the pbest position of a random particle (pbestrand) whose pbest is better than its own pbest, and a random position prand nearby. The four training techniques, respectively, play the roles of integration, manipulation, discovery, and jumping out of the regional optima attraction basins.

The four learning strategies allow each particle to deal with different circumstances independently. The learning equations corresponding to the four learning operators are given as follows for each particle k:

strategy a: learning from its pbest position

$$\text{exploitation}: v_k^d = \omega v_k^d + \eta \cdot r_k^d \cdot \left(pbest_k^d - x_k^d\right) \tag{2.7}$$

strategy b: learning from a random position nearby

$$\text{jumping out}: x_k^d = x_k^d + v_{avg}^d \cdot N\left(0,1\right) \tag{2.8}$$

strategy c: learning from the pbest of a random particle

$$\text{exploration}: v_k^d = \omega v_k^d + \eta \cdot r_k^d \cdot \left(pbest_{k\_nearest}^d - x_k^d\right) \tag{2.9}$$

strategy d: learning from the abest position

$$\text{convergence}: v_k^d = \omega v_k^d + \eta \cdot r_k^d \cdot \left(pbest_{gbest}^d - x_k^d\right) \tag{2.10}$$

The choice of which training option is best suited to a specific particle will depend on the local fitness environment in which it is located. It is presumed, however, that they do not know how the fitness landscape looks, although they have a priori knowledge of the fitness landscape.

2.5 Conclusion

This chapter introduced some fundamental knowledge of PSO, including the origin of PSO, the basic PSO algorithm, and the trajectory analysis of a particle. This chapter also reviewed the brief improved of PSO. In SLPSO, each particle has a set of learning strategies that are created through learning from four terms: its own historical best position, a random neighbor, the global best position, and a random position close-by, respectively. The four learning strategies have diverse properties that lead the particle to converge to the current global best position, exploit a local optimum, explore new promising areas and, respectively, jump from a local optimum.

Chapter 3

Control of Inverter-Based Distributed Generation

3.1 Introduction

Depending on the application of the distributed generator (DG), different controllers can be used to control the inverters that connected to an output filter of type L, LC or LCL. Filters are effective attenuation of switching harmonics. Nowadays, the LCL filter is frequently used in voltage source inverter (VSI) because of its advantages in terms of size and weight. However, LCL filters are complicated compared to the L filters as they possess a high number of equations and coupling terms which increases the complexity of the dynamics of the DG system. Moreover, due to the high resonance peak of LCL filters, their incorporation into VSIs requires the modification of the conventional controller.

The control of a DG is mainly designed in accordance with the grid code. The purpose of inner control is to ensure performance, the stability of the microgrid during both modes, to eliminate steady-state error and to improve the disturbances rejection and suppression harmonics. There are two categories of inner control scheme:

- multi-loops control that combine two or three control loops
- single control loop

Thus, many control techniques have been developed in recent years, these techniques vary from the simplest to very complex analytical approaches and so-called intelligent approaches, and each of control technique has advantages and disadvantages; it is very common to combine them to reap the benefits of each one.

Y. Jia *et al.* [44] proposed a resonant proportional regulator (PR) in the benchmark of two-phase alpha beta in order to track the AC current reference, likewise to avoid the strong coupling formed by two-phase transformation. H. Heo *et al.* [38] proposed the predictive active damping method to minimize resonance behavior while connecting to the grid. B. Yang *et al.* [11] proposed a control strategy predictive for the internal loop of the current and a fuzzy control strategy for the loop external voltage to eliminate the steady-state phase error between the current output and reference, and to compensate for errors caused by delays sampling and discretization calculations, with a fixed switching frequency. Y. Baek *et al.* [8] used predictive current control strategy based on the predictive direct power control strategy. But the disadvantage of this command is the mathematical approach, which is sensitive to parameter variations. The estimation of the parameters is done by the method of the least squares, it improves the precision of the control system

J. M. Espi *et al.* [22] presented an adaptive robust predictive current control (RPCC) for three-phase inverters connected to the grid. Error correction is performed by means of an adaptation strategy that works in parallel with the deadbeat algorithm, thus preserving the fast response characteristic of the prediction law. J. Hu *et al.* [43] presented a control strategy deadbeat predictive control of the power (DPC) with the improvement of the voltage vector sequences to VSI in a grid-connected mode. Y. Abdel-Rady Ibrahim Mohamed *et al.* [2] used the control deadbeat to minimize the prediction error (predict the action effect of the command) so that the reference current can be tracked correctly without any fault. L. Malesani *et al.* [59] discussed the robustness of this controller in which the estimation Line voltage enhances the robustness of the controller for inadequate parameters. L. Malesani *et al.* [60] proposed different methods and algorithms for controlling hysteresis to obtain a fixed switching frequency. Depending on the method used, complexity of the control unit

can be increased considerably. X. Dai *et al.* [19] presented an adaptive hysteresis band control algorithm featured the dynamic modulation of the hysteresis bandwidth.

S. Alepuz *et al.* [5] presented a simple and easy to implement approach for the control of a three-level inverter with neutral point (NPC) based on the linear–quadratic regulator (LQR) and Gain-Scheduling control techniques, these control techniques operate simultaneously in the regulator, which allows the control of all state variables, including state variables related to the voltages of the continuous bus P. Peltoniemi *et al.* [72]. X. Hao *et al.* [34] proposed a frequency integral resonant sliding mode controller (IRSMC). L. Shang *et al.* [85] presented an improvement in direct power control (DPC) based on the sliding mode controller when the grid voltage is unbalanced in order to achieve objectives of selective control, that is to say obtaining a balanced and sinusoidal current, by suppressing the ripples of the reactive power and the cancellation of the ripples of the power active. J. Hu *et al.* [45] proposed a control strategy that employs a non-linear sliding mode control to directly calculate the voltage of the converter needed to eliminate active and reactive power errors without involve all the transformation of synchronous coordinates.

T. Hornik *et al.* [41] proposed a design of the current regulator on the basis H∞ and repetitive control technique for inverters connected to the grid to reduce the THD of the current. The H∞ current regulator keeps a balance in focus neutral of the inverter and eliminates the current flowing through the capacitors in the continuous part. T. Liu *et al.* [93] proposed a control strategy for dampen the harmonics, the output current of the inverter is controlled by a PI regulator and the grid current is controlled by the repetitive controller (RC). D. Chen *et al.* [15] proposed an improved control system based on the repetitive control, for the three-phase inverters connected to the grid. The proposed system adopts $\frac{T_o}{6}$ as the delay time in synchronous reference frames with positive rotation and negative rotation for remove the $6n \pm 1$ harmonics. A. Asbafkan *et al.* [7] presented an adaptation of the frequency with a repetitive controller (RC), which is based on the internal model principle (IMP). T. Hornik *et al.* [74, 100] proposed a voltage regulator that is implemented for inverters connected to the grid based on H∞ and repetitive control based on the internal model principle, which leads to a very low THD with improved tracking performance.

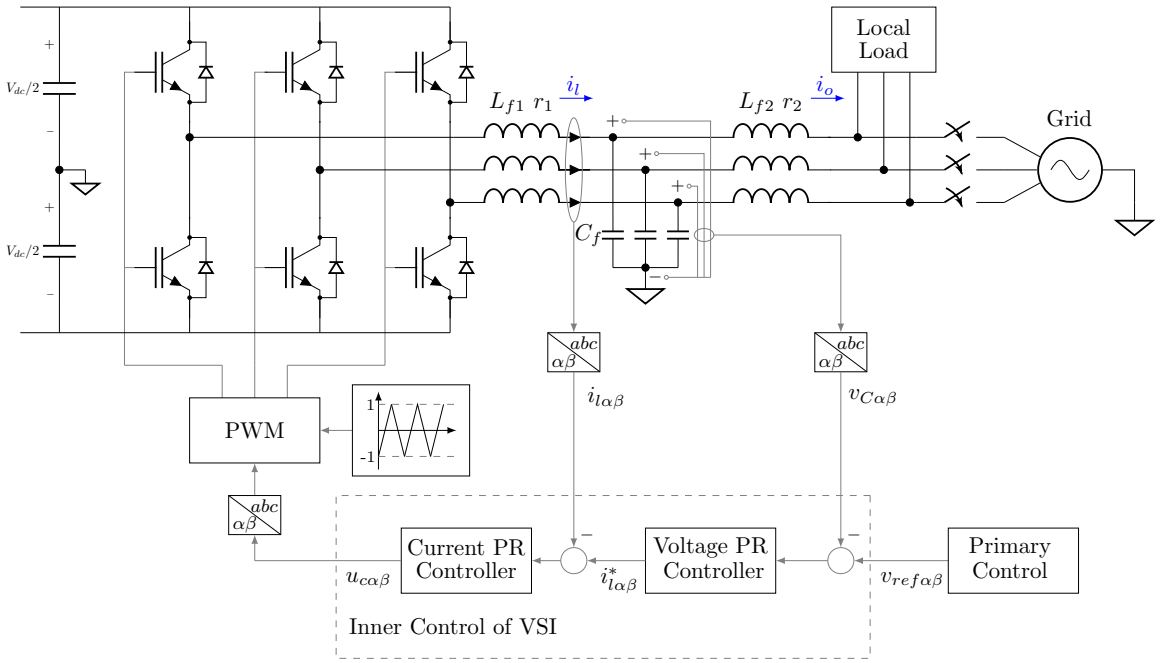

Fig. 3.1 Block diagram of the VSI with the cascaded control loops.

P.C. Loh *et al.* [55] proposed a new repetitive controller that can realize the rejection of several harmonics with a simple structure. The new controller has only been checked with an L filter in an inverter. T. Guofei *et al.* [30] used the closed loop double control method with a feed forward command to limit the resonance peak of the LCL filter and bring a gain high and quick response; repetitive control can provide the system with the ability to reduce harmonics in the grid and good robustness. D. Chen *et al.* [14] have proposed an improved repetitive control system specially designed with a finite impulse response (FIR). Cascading FIR filter with a traditional function delay can approximate the ideal repetitive control function of any report. C. Ma *et al.* [56] proposed a fuzzy logic controller (FLC) and a double PI-FLC mode controller to reduce overshoot and improve performance of pursuit error.

3.2 Cascaded Control of VSI

The cascaded control of VSI is based on cascaded control structure which consists of an outer voltage loop and an inner current loop (see Figure. 3.1). The advantages of this scheme are as follows:

- Achieves a low total harmonic distortion (THD) for the capacitor voltage v_{Cabc}.
- Keeps the inductor current i_{labc} within a safe limits.
- Maintain the same control scheme for different mode of operations (islanded or grid-connected mode).
- Improves more the disturbance rejection.

The role of outer voltage loop is to regulate the capacitor voltage v_{Cabc} to reference signal that is generated by the primary control, and also is responsible for setting the reference of the inner current loop, which in turn regulates the inductor current i_{labc}. The dynamics of the outer loop must be slower than those of the inner loop [96].

We transform the abc reference frame into $\alpha\beta$ stationary reference to get two independent single-phase systems by using Clarke transformation as shown in Figure. 3.2. The PR controllers are applied to get a better voltage regulation with less harmonics, and they can be expressed as follows [94, 63] :

$$G_v(s) = k_{pv} + \frac{k_{rv}s}{s^2 + \omega_c s + {\omega_o}^2} + \sum_{h=3,5,7} \frac{k_{hv}s}{s^2 + h\omega_c s + (h\omega_o)^2} \tag{3.1}$$

$$G_i(s) = k_{pi} + \frac{k_{ri}s}{s^2 + \omega_c s + {\omega_o}^2} + \sum_{h=3,5,7} \frac{k_{hi}s}{s^2 + h\omega_c s + (h\omega_o)^2} \tag{3.2}$$

where k_{pv} and k_{pi} are the proportional gains, k_{rv} and k_{ri} are the resonant gains at the fundamental frequency, k_{hv} and k_{hi} are the resonant gains at the h-harmonic, ω_c is the resonant bandwidth used to avoid the instability problems associated with the infinite gain, ω_o is the fundamental frequency. From the block diagram of Figure. 3.2 with using Mason's theorem [77], the closed loop transfer function (CLTF) of the inner current loop and outer voltage loop of the α-coordinate can be expressed by:

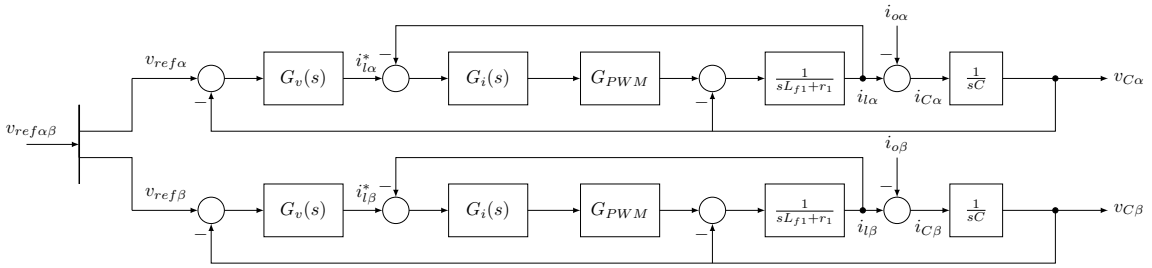

Fig. 3.2 Block diagram of the cascaded control loops in $\alpha\beta$-coordinates.

$$\begin{aligned} i_{l\alpha}(s) &= \frac{G_i(s)\,G_{PWM}(s)}{Z_l(s)+G_i(s)\,G_{PWM}(s)} i^*_{l\alpha}(s) - \\ &\quad \frac{1}{Z_l(s)+G_i(s)\,G_{PWM}(s)} v_{C\alpha}(s) \end{aligned} \tag{3.3}$$

$$\begin{aligned} v_{C\alpha}(s) &= \frac{G_{ol}(s)}{Z_C(s)+Z_l(s)+G_{in}(s)+G_{ol}(s)} v_{ref\alpha}(s) \\ &\quad -\frac{Z_C(s)\,(Z_l(s)+G_{in}(s))}{Z_C(s)+Z_l(s)+G_{in}(s)+G_{ol}(s)} i_{o\alpha}(s) \end{aligned} \tag{3.4}$$

Where

$$G_{ol}(s) = G_v(s)\,G_i(s)\,G_{PWM}(s)\,Z_C(s)$$

$$G_{in}(s) = G_i(s)\,G_{PWM}(s)$$

$$G_{PWM}(s) = \frac{V_{dc}/2}{1+1.5T_s s}$$

$Z_l = sL_{f1} + r_1$, $Z_C = \frac{1}{sC}$ and G_{PWM} is the transfer function of the PWM delay, T_s is the sampling time which equals to $\frac{1}{f_s}$. The same model can be developed in β-coordinate. In section 4.4 we discus how to tune optimally the parameters of PR controllers.

3.3 Enhancing the Power Quality of an Islanded Microgrid

In recent years, there has been growing interest in integrating the renewable energy sources (RESs) into the conventional power grid to confront the global warming. This opens a new technological paradigm in the power system which allows the distributed generations (DGs). Over the next few years, the renewables will become an obligation to cope with the increas-

Table 3.1 Inverters parameters with their output impedances

Parameter	Symbol	VSI_1	VSI_2	VSI_3	Units
Inverter-side filter inductor	L_{f1}	1.8	1.8	1.8	mH
Parasitic resistor 1	r_1	0.03	0.03	0.03	Ω
Grid-side filter inductor	L_{f2}	1.8	1.8	1.8	mH
Parasitic resistor 2	r_2	0.03	0.03	0.03	Ω
Filter capacitor	C_f	35	35	35	μC
DC voltage	V_{dc}	650	650	650	V
PWM switching frequency	f_s	10	10	10	kHz
Output impedance	Z_o	$0.7,\ 2.6$	$0.5,\ 1.9$	$0.8,\ 1.6$	Ω, mH
Apparent power rating	S	1	2	3	kVA

ing demand [101] .

However, the direct connection of these sources to the grid cause significant disturbances on the supplied voltage, since they fluctuate and variable. To prevent this problem, they need to operate in parallel with energy storage systems (ESSs) that compensate their intermittence and make the injected power more smooth [17]. Hence, the microgrid was introduced in the literature, as a local electrical distribution grid which consists of multiple units of RESs and ESSs, as well as local loads. The microgrid is interfaced with the main grid via point of common coupling (PCC) and is able to operate either in islanded or grid-connected mode. In the islanded mode, the microgrid operates autonomously where the local load is fully supplied by local DGs (RESs and ESSs), whereas in the grid-connected mode it connects to the main grid, in order to exchange power.

The RESs have heterogeneous power forms, which some of them are variable AC frequency like wind turbines, others are AC high frequency like small hydro turbines and the rest are DC sources such as photovoltaic. These sources need to be accommodated to the power grid through power electronics devices which convert the high and variable frequency to DC using AC/DC rectifier, and from DC sources to synchronous AC using inverters (DC/AC). Since there are multi-units of DGs, the inverters are operating in parallel and each one is connected to the common bus via LCL filter and line impedance that represents a physical distance.

However, this may cause power quality issues especially when the microgrid is operating in

the islanded mode, where the inverters ought to supply the local loads. The power quality is related to the voltage waveform at the load's terminal (PCC voltage), while the current is determined by Ohm's law. Therefore, any variation in amplitude and frequency, or distortion in the voltage's waveform affects directly the power quality consumed by the local loads.

In our previous works [105, 107, 106], we developed a control scheme based on the hierarchical structure to maintain the PCC voltage's amplitude and frequency in their nominal values. In order to regulate the capacitor voltage of each inverter, we used an inner control loop based on Proportional Resonance controllers (PR), where the objective is to deliver a perfect sinusoidal waveform at capacitor terminal. In other hand, when the paralleled inverters fed a nonlinear load, a current harmonics are presented and they lead to drop voltage at the output impedances and the line impedances which cause distortion to the PCC voltage. Hence, a poor power quality is absorbed by the local nonlinear load.

Several control techniques for suppression the voltage harmonics have been presented in the literature. In [62], a capacitive virtual loop is proposed to compensate the harmonics caused by the output inductance. The output of the virtual capacitor is added to the reference of the inner control. In [6], the authors inspired from the previous idea with considering the delays caused by measuring, filtering and computation.

In this work, we intend to enhance the power quality of an islanded microgrid by compensating harmonics of the PCC voltage. We propose an optimal design of the virtual impedance and the PR controllers at a selected harmonics (3rd, 5th, 7th, 9th, 11th, and 13th).

3.3.1 Power quality issues

Power quality is a term used to describe the electric power delivered to the consumer which it can be expressed by the ratio of the actual power consumed and the desired power of the consumer. Since the power system suppliers are mainly voltage sources instead of current sources, thus, the power quality is referred to the quality of voltage waveform at PCC. This means any change in its amplitude, frequency or waveform will diminish the power quality.

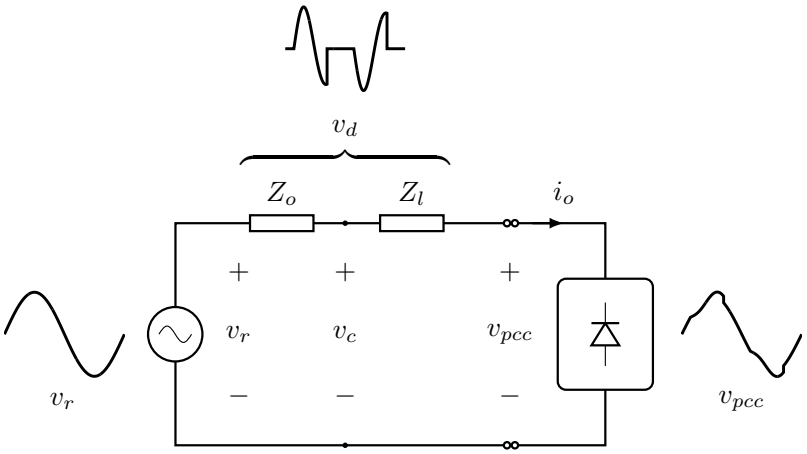

Fig. 3.3 Model of a voltage source inverter.

Poor power quality can affect the efficiency and the proper function of the electrical devices or even a dysfunction.

In this work, we focus on degradation caused by harmonics that appear when the voltage source inverters (VSIs) supply a nonlinear load. The presence of latter load produces harmonics in the injected current of each inverter, which in turn distort the PCC voltage waveform due to the LCL filter and the line impedance (see Figure 3.5). These harmonics cause overloading, overheating and increasing power losses, as well as they, may cause resonances that lead to stability problems in the microgrid [101].

Figure 3.6 3.3. shows an inverter modeled as an ideal voltage source in series with output impedance and line impedance. The output impedance depends on DC link, LCL filter, and control parameters of the inner loop; this is coved in next section. The voltage source generates an ideal sinusoidal voltage to supply a nonlinear load. By using the Kirchhoff's Voltage Law, the PCC voltage is expressed as:

$$v_{pcc} = \overbrace{v_r - \underbrace{Z_o\left(s\right) i_o}_{v_d}}^{v_c} - Z_l\left(s\right) i_o \tag{3.5}$$

Where v_c is the output voltage across the inverter's capacitor, v_r is the voltage reference generated by the primary control, v_{pcc} is the voltage at the load's terminal and i_o is the output current flowing through the grid-side inductor.

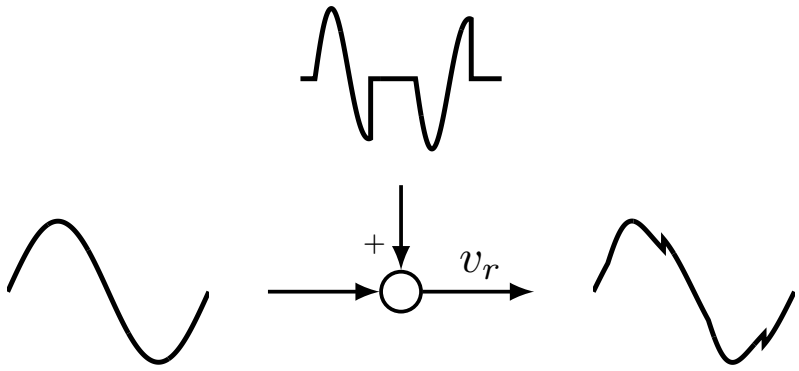

Fig. 3.4 Regenerate the reference voltage by adding a specified harmonics.

It is clear that the current i_o causes harmonic voltage drops v_d on the output impedance Z_o and line impedance Z_l when it contains harmonics. These drops lead to voltage distortion at PCC (as shown in Figure 3.3), which degrades the voltage quality, therefore, a poor power quality is absorbed by the nonlinear load. For the sake of improving the power quality, we aim to provide a pure voltage sinusoidal waveform at PCC through changing the voltage reference v_r to contain the ideal sinusoidal voltage plus specified harmonics in order to get canceled by the voltage drops of the impedances (see Figure 3.4).

3.3.2 Inner control loop

In this section, we give details of the control scheme that regulates the inverter's capacitor voltage with at the same time it compensates the harmonics caused by the output impedance. In addition to that, we present another loop based on virtual impedance which is used to redraw the reference voltage generated by the primary control in order to mitigate the harmonics caused by the line impedance. The parameters of the controllers and the virtual impedance are tuned in such a way to minimize an objective function.

PR controllers

The control scheme of the inverter is based on cascaded control structure which consists of an outer voltage loop and an inner current loop. The main advantage of this scheme is to achieve a low total harmonic distortion (THD) for the capacitor voltage v_c. Therefore, the

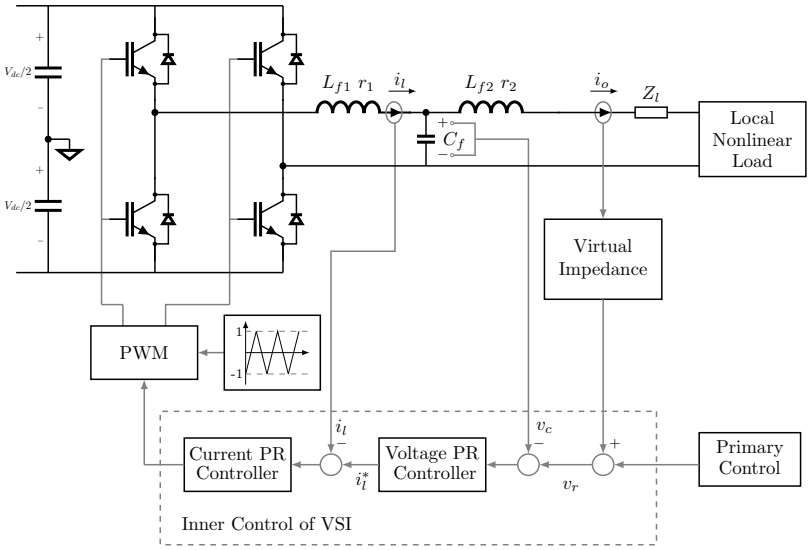

Fig. 3.5 VSI with the inner control loops.

effects of the output impedance on the v_c are compensated. The role of outer voltage loop is to regulate the v_c to reference signal, and also is responsible for setting the reference of the inner current loop, which in turn regulates the inductor current i_l (see Figure 3.5).

Proportional-resonant (PR) controllers are applied to both control loops in order to get a better voltage regulation with less harmonics, and they can be expressed as follows:

$$G_v(s) = k_{pv} + \sum_h \frac{k_{hv} s}{s^2 + \omega_c s + (h\omega_o)^2}$$
$$G_i(s) = k_{pi} + \sum_h \frac{k_{hi} s}{s^2 + \omega_c s + (h\omega_o)^2}$$

where k_{pv} and k_{pi} are the proportional gains, k_{hv} and k_{hi} are the resonant gains at the h-harmonic. The selective harmonics are up to 13th ($h = \{1, 3, 5, 7, 9, 11, 13\}$) for both current and voltage which are enough to be considered in the most cases. ω_c is the resonant bandwidth used to avoid the instability problems associated with the infinite gain, ω_o is the fundamental frequency (see Table 3.2). From the block diagram of Figure 3.6, the closed loop transfer function (CLTF) of the outer voltage loop can be expressed by:

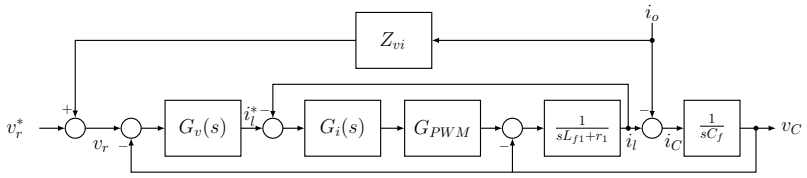

Fig. 3.6 Block diagram of the VSI with the inner control loops.

$$\begin{aligned} v_c(s) &= \frac{G_{ol}(s)}{Z_c(s)+Z_l(s)+G_{in}(s)} v_r(s) \\ &\quad -\frac{Z_c(s)\left(Z_l(s)+G_i(s)\right)}{Z_c(s)+Z_l(s)+G_{in}(s)} i_o(s) \end{aligned} \tag{3.6}$$

Where

$$G_{ol}(s) = G_v(s)\, G_i(s)\, K_{PWM} Z_c(s)$$
$$G_{in}(s) = G_i(s)\, K_{PWM} + G_{ol}(s)$$
$$K_{PWM} = \frac{V_{dc}}{2}$$
$$Z_l = sL_{f1} + r_1, Z_C = 1/sC_f$$

We can rewrite (3.6) to become:

$$v_c = G_{vv}(s)\, v_r(s) - Z_o(s)\, i_o(s) \tag{3.7}$$

It is clear that the output impedance Z_o depends on the PR controllers, thus, its effects can be attenuated especially in the selected harmonics. By using the values of PR controllers presented in Table 1, the G_{vv} has nearly unity gain and zero phase in the selected harmonics and this means that v_c can follow the voltage reference when it contains the harmonics of h.

Virtual impedance

Considering the real model of the inverter with PR controllers, the PCC voltage can be written as:

$$v_{pcc} = G_{vv}(s)\, v_r - Z_o(s)\, i_o - Z_l(s)\, i_o \tag{3.8}$$

From Figure 3.6, v_r is expressed as follows:

$$v_r = v_r^* + Z_{vi}(s)\, i_o \tag{3.9}$$

Where $Z_{vi}(s)$ is the virtual impedance, v_r^* is a sinusoidal voltage with fundamental frequency and it is generated by the primary control. By substituting (3.9) into (3.8) gives:

$$\begin{aligned} v_{pcc} = {} & G_{vv}(s)\, v_r^* + G_{vv}(s)\, Z_{vi}(s)\, i_o \\ & - Z_o(s)\, i_o - Z_l(s)\, i_o \end{aligned} \tag{3.10}$$

Assume that the harmonics of output current i_o at higher than 13th are negligible next to the selected ones, and as discussed in the previous subsection, at the selected harmonics, Z_o attenuates and G_{vv} approximately equals to one, hence, the equation (3.10) becomes:

$$v_{pcc} = v_r^* + Z_{vi}(s)\, i_o - Z_l(s)\, i_o \tag{3.11}$$

In order to mitigate the harmonics that come from the line impedance, we should design the virtual impedance according to the following equation:

$$Z_{vi}(s)\, i_o - Z_l(s)\, i_o = 0 \tag{3.12}$$

Assume that the line impedance is a resistance plus an inductance and i_o is equal to:

$$i_o = \sum_h I_h \sin\left(h\omega_o t + \phi_h\right) \tag{3.13}$$

The drop voltage at the line impedance can be written as:

$$v_l = R_l i_o + \sum_h hL_l \omega_o I_h \cos\left(h\omega_o t + \phi_h\right) \tag{3.14}$$

Supposed that the virtual impedance is a resistance plus a capacitance, then the virtual voltage equals to:

$$v_{vi} = R_{vi} i_o - \sum_h \frac{1}{hC_{vi}\omega_o} I_h \cos\left(h\omega_o t + \phi_h\right) \tag{3.15}$$

In order to verify the equation (3.12), the virtual resistance and capacitance must be equal to:

$$R_{vi} = R_l \tag{3.16}$$

$$C_{vi} = \frac{1}{L_l \left(h\omega_o\right)^2} \tag{3.17}$$

C_{vi} depends on the harmonic number h which means that each hth current harmonic needs to be multiplied by its own gain. Therefore, each current harmonic needs to be extracted by using the resonance filter which is described as follows:

$$G_{rh}\left(s\right) = \frac{\omega_r s}{s^2 + \omega_r s + \left(h\omega_o\right)^2} \tag{3.18}$$

Where ω_r is the resonant bandwidth. The transfer function of the virtual impedance can be expressed as follows:

$$Z_{vi}\left(s\right) = R_l - \sum_h \frac{L_l \left(h\omega_o\right)^2 \omega_r}{s^2 + \omega_r s + \left(h\omega_o\right)^2} \tag{3.19}$$

Optimal tuning

The PR controller parameters, the resonant bandwidth ω_c and ω_r are designed by solving an optimization problem in order to find their optimal values. The optimization problem is defined as minimization of a fitness function. The concept stands on evaluating the fitness function after each adjustment of the optimization vector until we find its smallest possible value, which we assume that corresponds to the optimal parameters. The optimization problem is defined as the THD of two cycles of the v_{pcc} at steady state. It is described as follows:

$$\begin{aligned} &\underset{\theta}{\text{minimize}} \quad THD\left(v_{pcc}\right) \\ &\text{subject to} \quad 0 < \theta_i \leq \theta_{imax},\ i = 1, \ldots, 18. \end{aligned} \tag{3.20}$$

Where $\theta = [k_{pi}\ k_{1i}\ k_{3i}\ k_{5i}\ k_{7i}\ k_{9i}\ k_{11}\ k_{13i}\ k_{pv}\ k_{1v}\ \ k_{3v}\ k_{5v}\ k_{7v}\ k_{9v}\ k_{11v}\ k_{13v}\ \omega_c\ \omega_r]^T$ and θ_{max} is the upper bound of the parameters which are determined by analyzing the bandwidth of $Gvv(s)$ for not exceed the PWM switching frequency f_s.

To solve this problem, we apply a meta-heuristic algorithm which is based on PSO (Particle Swarm Optimization) and is called SLPSO (Self-Learning Particle Swarm Optimizer).

Table 3.2 Microgrid control system parameters

Parameter	Symbol	Value
Microgrid system		
Fundamental frequency	ω_o	$2\pi \cdot 50$ rad/s
Nominal RMS voltage	E^*	220 V
Inverter-side filter inductance	$L_{f1,2}$	1.14 mH
Parasitic resistance	$r_{1,2}$	0.05 Ω
Filter capacitor	C_f	2 μC
DC voltage	V_{dc}	733 V
Line impedance of VSI_1	Z_{l1}	0.45,1.5 Ω, mH
Line impedance of VSI_2	Z_{l2}	0.65,1.8 Ω, mH
PWM switching frequency	f_s	10 kHz
PR, VI resonant bandwidth	ω_c, ω_r	1.4, 16.4
Voltage PR k_{pv}, k_{hv}		0.5, 199, 80, 26, 9, 52, 10, 199
Current PR k_{pi}, k_{hi}		0.2, 98, 98, 99, 99, 99, 98, 99

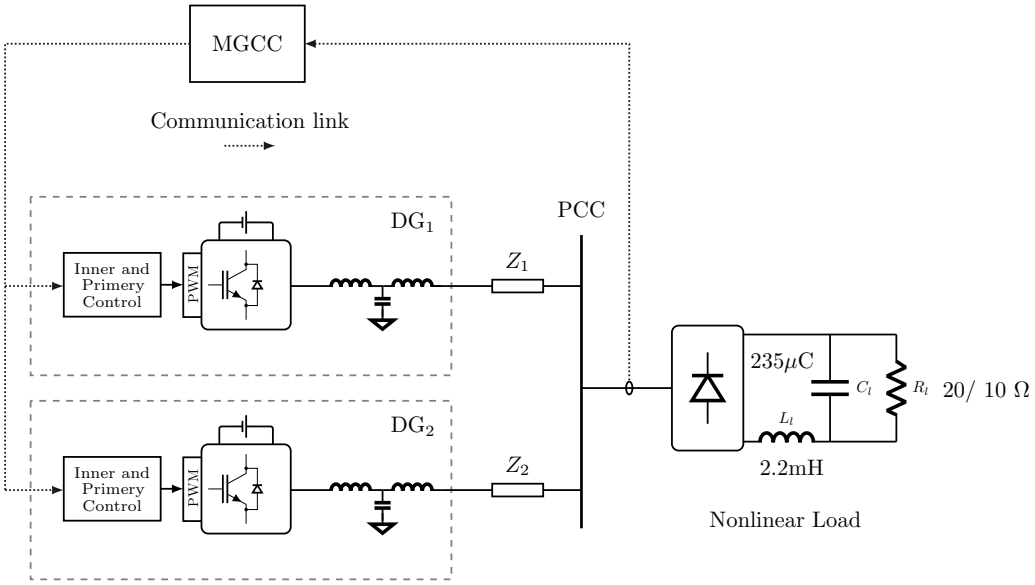

Fig. 3.7 Single line diagram of the microgrid setup.

3.3.3 Simulation results

This section demonstrates the effectiveness of the virtual impedance developed in the previous Section. The considered system consists of two inverters operated in parallel and supplying a single-phase uncontrolled rectifier loaded with LC filter and a variable resistor (see 3.7). The simulation was carried out in MATLAB/Simulink environment.

There are two case studies, first when the virtual impedance loop is deactivated and second when it is activated. Figure 3.8 shows THD of the PCC voltage in both cases. In time range from $0.3s$ to $3s$, the THD of the first case is 8.3% while in the second case the THD decreased until the settled value of 1.6% with respond time of $0.25s$ which the reduction ratio is about 80%.

Figure 3.10 shows a comparison between the cases which presents the harmonic component of two cycles ($2.96s - 3s$) of PCC voltage relative to the nominal amplitude. This figure shows clearly that the virtual impedance loop significantly reduces the selected harmonics. Moreover, the virtual impedance performs very well when the power demand is suddenly increased ($t = 3s$), which demonstrates the robustness of the proposed loop.

Figure 3.11 shows the absorbed active and reactive power by the nonlinear load of both cases.

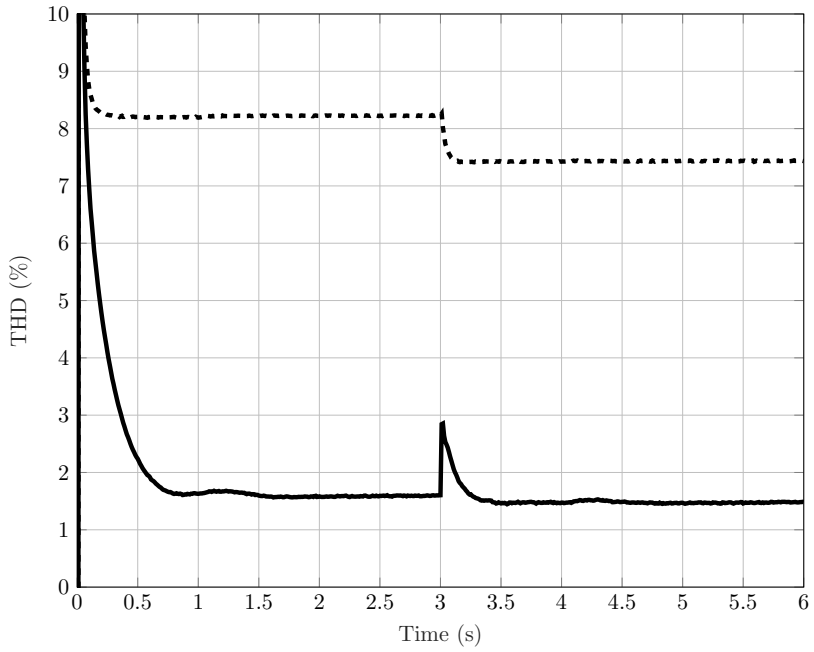

Fig. 3.8 The THD of the PCC voltage with (solid line) and without (dashed line) the virtual impedance loop.

If we give a close look at $t = 2$ for instance, we notice that the load consume more active power in the first case then its desired, this due to the significant THD at that time which confirm the claim about the overloading and the effects on the proper function of the second section. And the same thing for the reactive power. Whereas, in the second case when the virtual impedance loop is acting, the nonlinear load nearly follows its desired for both active and reactive power.

3.4 Conclusion

In this chapter, a control scheme of a distributed generator connected to loads by the LCL filter is proposed. The method of controlling the two cascade loops was presented as well as the design of the virtual impedance for enhancing the power quality of microgrid during islanded mode. This technique is based on PR controllers and a virtual impedance loop in order to face the drop voltage caused by the line impedance. The performed results prove the performance and the robustness of the proposed scheme.

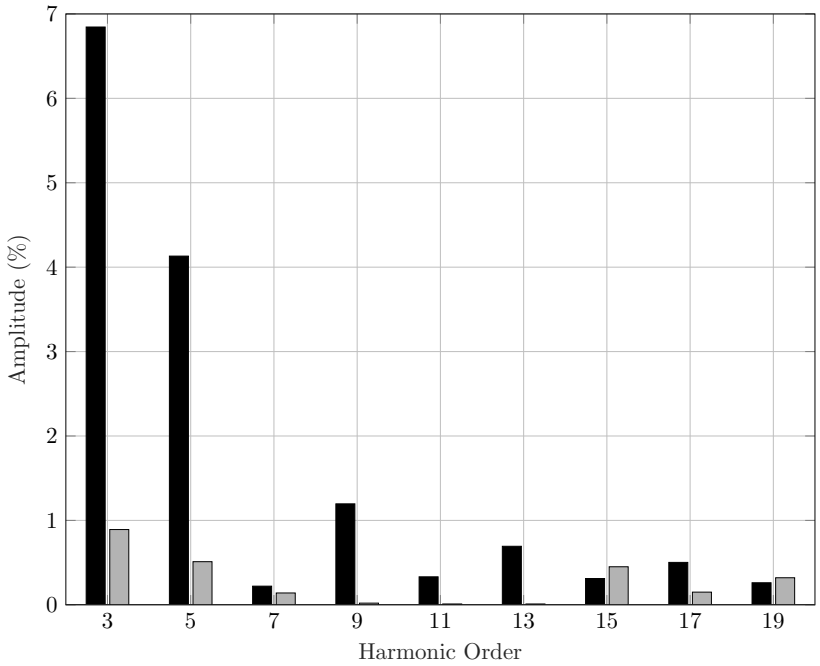

Fig. 3.9 PCC voltage harmonic content with (gray) and without (black) the virtual impedance loop.

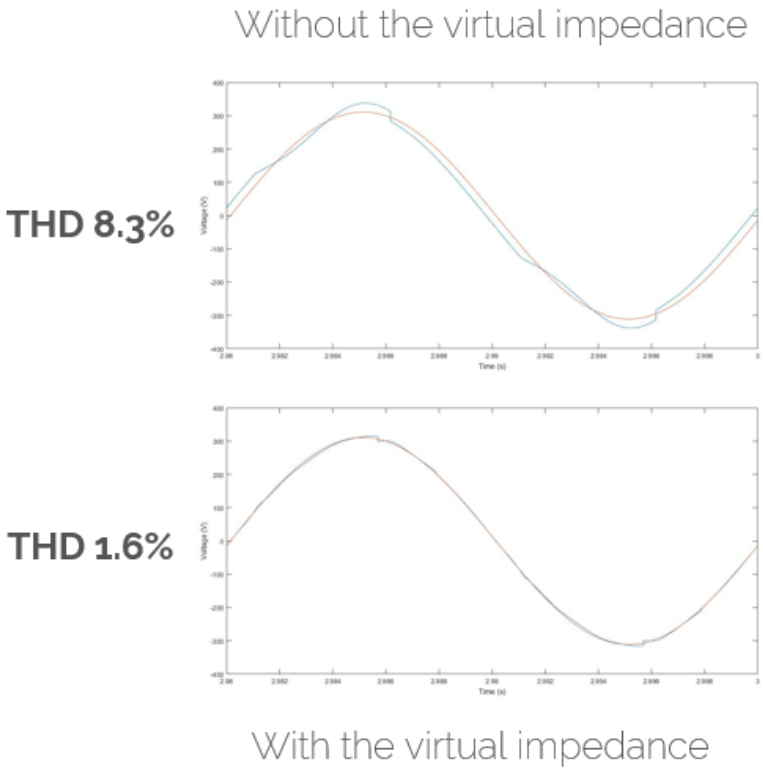

Fig. 3.10 PCC voltage harmonic content with and without the virtual impedance loop (the reference is in red).

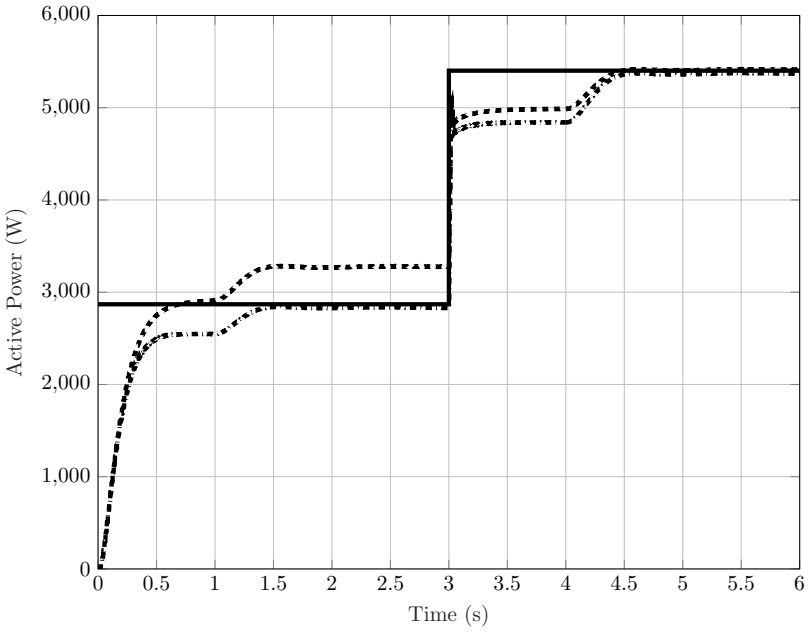

(a)

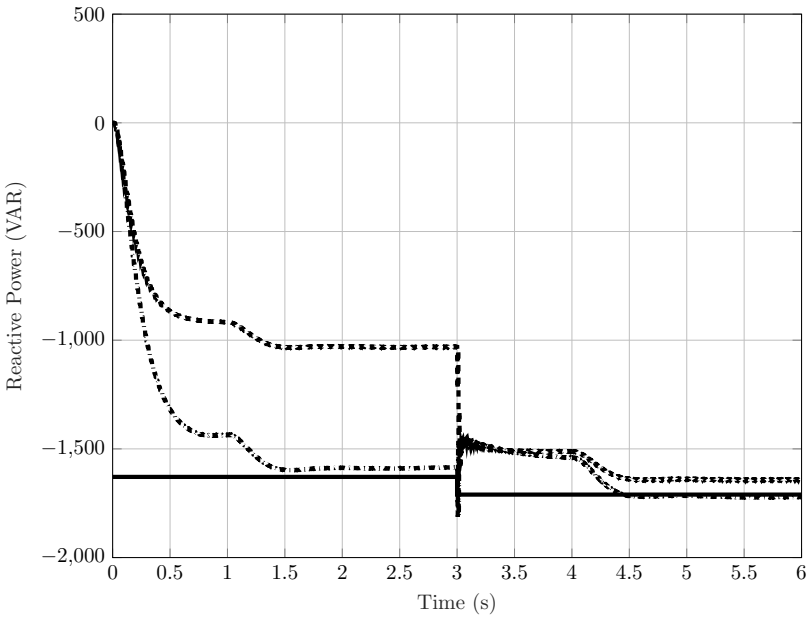

(b)

Fig. 3.11 Active and reactive power consumed by the load. Solid line for the desired power. Dash-dot line when the virtual impedance loop is activated. Dashed line when it is deactivated

Chapter 4

Decentralized Control of Paralleled Distributed Generations

4.1 Introduction

The increasing integration of DGs into the electrical grid poses many challenges in term of performance, robustness, and stability of microgrids. These challenges are faced by ensuring proper regulation of microgrid voltage that allows the achievement of a simultaneous sharing of active and reactive power among the different DGs that are connected in parallel. To meet these requirements, several research works have been conducted to power-sharing control. These strategies are based on one or more combinations of power (active and reactive), voltage amplitude, frequency, phase angle. According to experimental results, the technique so-called droop control has shown an excellent power sharing of several DGs operation in parallel, and also it allows the connection/disconnection of the microgrid to/from the main grid.

However, the conventional droop control is based on a highly inductive electrical grid with a high ratio (X/R) of line impedance. In the case of low voltage microgrid, the impedance lines are mainly resistive with a low ratio (X/R) of line impedance. In the literature, there is a lot of research works that attempted to propose a control strategy to achieve a high

performance of a microgrid. This section quotes some jobs used for active power sharing and reactive power sharing to ensure an optimal state of a microgrid.

M. C. Chandorkar *et al.* [13] used a controller from Conventional droop for control and sharing of active power in the presence a variation of the load. U. Borup *et al.* [12] presented a method of sharing power to eliminate the circulating harmonic currents between DGs in the presence of non-linear load. However, the dynamic performance of the system is not improved. J. M. Guerrero *et al.* [26] proposed an improved statics controller capable of modifying the response dynamic system connected in parallel by correctly adjusting the parameters of gain of the control system. According to J. M. Guerrero *et al.* [27] in extreme situations, the poor sharing of reactive power can cause severe reactive power flows between DG units and can cause instability of the system. Y. A. I. Mohamed *et al.* [65] presented a decentralized adaptive control system based on the droop control in order to adjust the dynamic performance of power sharing without affecting the gain of droop. S. Ahn *et al.* [4] studied an active power control strategy based on two algorithms: 1) output power control unit (UPC) and 2) feed rate (FFC) in order to share the power under conditions of complex tasks. Y. A. I. Mohamed *et al.* [67] presented optimized droop control to improve the dynamic stability of active power sharing.

Y. A. I. Mohamed *et al.* [66] achieved high performance of disturbance rejection against disturbances of voltage when sharing active power. A. Kahrobaeian *et al.* [46] made improvements to some control methods of the power of the impedance resistive/inductive power supply. A. Ghazanfari *et al.* [25] presented a hierarchical strategy for the management of active power. Although the sharing of active power is achieved microgrid is ensured, the complex feed impedance and the production costs of the microgrid are not considered. So the economic problem is introduced in the hierarchical control, the criterion of active power must be based on the cost of production of the microgrid instead of a simple or equivalent proportional relationship based on generator evaluations. G. Chen *et al.* [16] proposed a nonlinear cost-based system. I. U. Nutkani *et al.* [68] presented two cost-based linear schemes, the common goal of which is to autonomously reduce the total cost of production (in English THC) of microgrid, while preserving the simplicity of traditional droop. H. Han textitet

al. [33] when all DG units operate at the same frequency in equilibrium conditions, the active power can be well regulated with improvement of the droop control systems, but the reactive power sharing still remains poor and the harmonics appear in the DG units when the Power impedances are unequal.

To ensure the sharing of reactive power, different methods of droop control have been proposed, these methods include three main categories:

1. Methods based on improved droop control: J. He *et al.* [35] presented a control strategy to share the reactive power with precision, where the disruption of the active power is adopted to identifying the reactive power sharing error and it is eliminated using a term slow integral. However, the signal injection method deteriorates the quality of power and affects the stability of the system. H. Mahmood *et al.* [58] presented a droop control adaptive to share reactive power. The effect of power supply impedances inconsistent is compensated for by adaptive droop coefficients. The method is immunized against communication delay but nonlinear charges and asymmetric are not considered in this study.

2. Methods based on improved virtual impedance: In addition to the improved droop control, the control methods based on virtual impedance or enhanced virtual impedance have been proposed by several researchers K. De Brabandere *et al.* [20], M. Mao *et al.* [61], P. Sreekumar *et al.* [91], H. Han *et al.* [32], M. Savaghebi *et al.* [83] for power sharing of active and reactive. Although virtual inductive impedance can improve the ability to sharing reactive power under the condition of unequal power impedances, the reactive power cannot be shared accurately when the loads are no linear and unbalanced in an autonomous microgrid. H. Mahmood *et al.* [57] proposed an Energy Management System (EMS) to distribute power reactive to DG units according to their own capabilities, the total demand of the loads and coping factors, but the coping factors are difficult to get. J. He *et al.* [37] have proposed a reinforced virtual impedance control strategy to share power reactive in a standalone microgrid with unequal power impedance, where impedance virtual is used at fundamental and harmonic frequencies. However, a sharing poor reactive power can occur in a three-phase converter with non-linear

loads. Y. Zhu *et al.* [103] have adopted a virtual resistance-based control strategy to share the reactive power under unequal line impedances, non-linear loads and unbalanced. However, if the feeder or load is disconnected, the microgrid would be unstable, which limits its practical applications.

3. Hierarchical control strategies: Since it is difficult to achieve the sharing of reactive power by methods improved virtual impedance in complex microgrids, the control strategy hierarchy has been proposed to ensure performance. These strategies are used as supplements to conventional droop controls and impedance methods Virtual. Thus, the frequency and voltage amplitude of the microgrid can be restored to their nominal values, while sharing the active and reactive powers. M. Hamzeh *et al.* [31] proposed a self-adjustment strategy based on the hierarchical control. This strategy uses adaptive droop control to share the reactive power and a secondary controller to restore the amplitude of voltage and frequency at a nominal value. Y. Zhu *et al.* [104] presented a control method that combines the central microgrid controller (MGCC) and droop control to share reactive power. MGCC is used to calculate average reactive power and regulate reactive power references corresponding to DG units. However, the reactive power can be seriously affected by the delay in communication. D. Wu *et al.* [98] proposed the distributed strategy that integrates the current control mode (CCM) and voltage control mode (V CM) to share the active and reactive. M. Falahi *et al.* [23] added droop control and reverse droop to the CCM and VCM controllers to regulate the reactive power. M. Savaghebi *et al.* [82] used the sequence positive power to generate the reference voltage and the negative sequence of reactive power for the compensation of the voltage imbalance. H. Jinwei *et al.* [36] proposed an improved power sharing method to share the reactive power of autonomous microgrid, where the droop control of the Frequency is used to compensate the reagent, the imbalance. J. W. Simpson-Porco *et al.* [90] proposed an algorithm optimized based on the theory of graphs to achieve the sharing of reactive power in the condition where the impedance of the power lines is unequal.A. Milczarek *et al.* [64] presented a programming algorithm to ensure the safety of the equipment and to achieve a simultaneous and accu-

rate sharing of the reactive power. V. Kekatos *et al.* [47] have presented a stochastic reactive power management strategy. This strategy is completely distributed. According to Q. Li *et al.* [54] an uncontrollable renewable energy source is environmentally sensitive outside, an agent-based method is presented to stabilize the active powers and reactive.

The study of the literature reveals that even though a great deal of research exists, the existing approaches to droop control do not generally guarantee the sharing of desired reactive power. This problem is difficult and remains an open problem because, unlike the frequency, the voltage is not fixed along the microgrid. Another question important that has not yet been fully studied in the technical literature is a rigorous analysis of the transient stability of microgrid interfaced by converters, due to changes in load, non-linear loads, defects, a transition of mode connected to the network, and vice versa [80]. Although extensive research has been conducted on the development of controllers for microgrids, there are still several challenges to overcome, among them: (1) robustness to parametric uncertainties of the filter connected to the output of the inverter and the lines of connection with the microgrid, (2) the need for advanced control design strategies with a decentralized structure, (3) the plug-and-play (PnP) functionality of the generator distributed, and (4) low complexity voltage controllers.

4.2 Improved universal droop control

The primary control adopted in this thesis is based on the universal droop control that was developed by Q.-C. Zhong [102], which we have improved it by introducing a derivative term to enhance the transition response and a hybrid term to distinguish between different mode of operation.

The primary control can be described as:

$$\dot{E} = \left(K_e \left(E^* - V_{pcc} \right) - n \left(P - P^* \right) - n_d \frac{d \left(P - P^* \right)}{dt} \right) \left(\overline{g}_c + g_c n_g \right) \tag{4.1}$$

$$\omega = \left(\omega^* + m \left(Q - Q^* \right) + m_d \frac{d \left(Q - Q^* \right)}{dt} \right) \left(\overline{g}_c + g_c m_g \right) \tag{4.2}$$

where E and ω are amplitude (RMS) and frequency of the capacitor voltage of VSI, respectively; E^* and ω^* are their nominal values. P^* and Q^* are the desired active and reactive power to be injected during the grid-connected mode, normally are set to zero in islanded mode. V_{pcc} is the amplitude (RMS) of the voltage at PCC, n and m are the droop coefficients, n_d and m_d are the derivative droop coefficients of the active and reactive power, respectively. K_e is an amplifier used to maintain the PCC voltage within a desired range and is chosen the same for all VSIs operated in parallel (see Table 4.2). n_g and m_g are used to improve the response and the stability of the microgrid during grid-connected mode. g_c is a hybrid variable which can be written as:

$$g_c = \begin{cases} 1 \quad if \quad \text{Microgrid operates in grid-connected mode} \\ 0 \quad if \quad \text{Microgrid operates in islanded mode} \end{cases} \tag{4.3}$$

$$\overline{g}_c = 1 - g_c \tag{4.4}$$

The instantaneous active and reactive power of VSI that is injected into the microgrid common bus is expressed in the $\alpha\beta$ stationary reference frame as follows [73]:

$$p(t) = v_{pcc\alpha} i_{o\alpha} + v_{pcc\beta} i_{o\beta} \tag{4.5}$$

$$q(t) = v_{pcc\beta} i_{o\alpha} - v_{pcc\alpha} i_{o\beta} \tag{4.6}$$

where v_{pcc} and i_o are voltage at PCC and the output current of the VSI, respectively. The average power of P and Q in Figure. 4.1 is calculated by integrating (4.5) and (4.6) over one fundamental cycle T and is described as:

$$P = \frac{1}{T} \int_{t-T}^{t} p(t) dt \tag{4.7}$$

$$Q = \frac{1}{T} \int_{t-T}^{t} q(t) dt \tag{4.8}$$

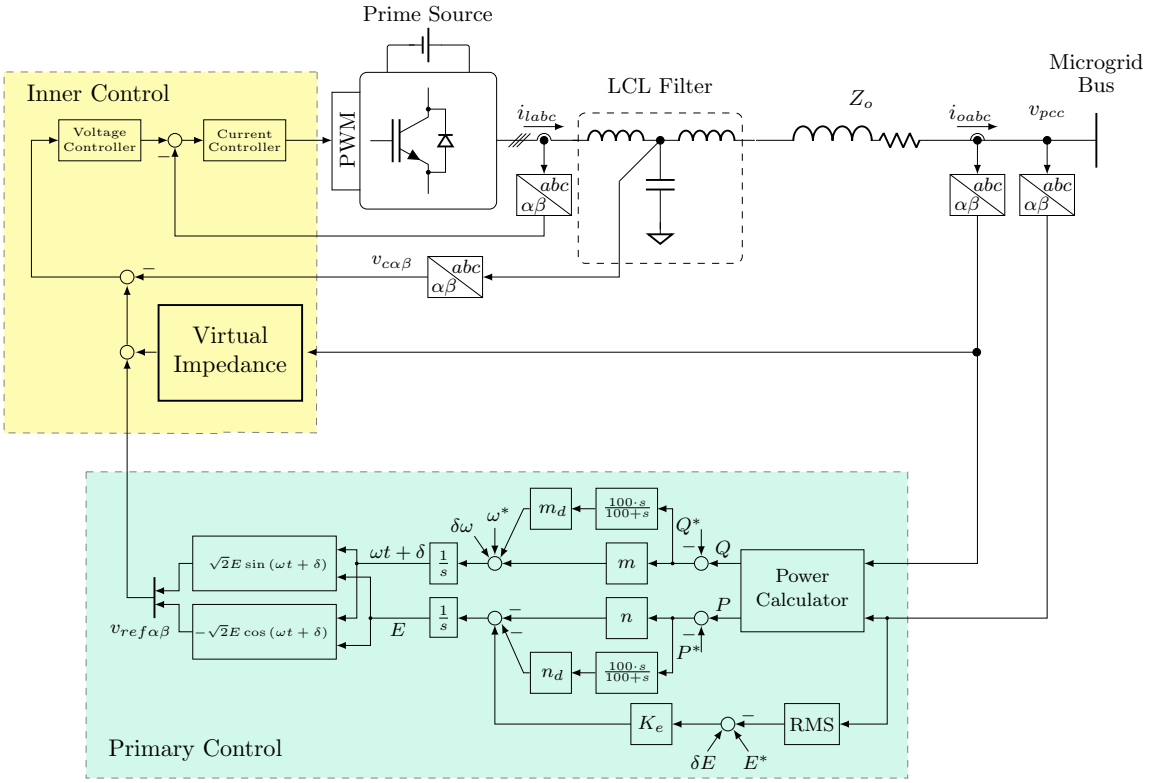

Fig. 4.1 Block diagram of the primary control in $\alpha\beta$-coordinates.

By applying the Laplace transformation to (4.7) and (4.8), we obtain the following equations [3]:

$$P(s) = F(s)p(s) \tag{4.9}$$

$$Q(s) = F(s)q(s) \tag{4.10}$$

where $F(s)$ is the transfer function of the integration filter and is expressed as follows:

$$F(s) = \frac{1}{Ts}\left(1 - e^{-Ts}\right) \tag{4.11}$$

The expressions from (4.5) to (4.11) are used to construct the power calculator of the Figure. 4.1 (see Figure. 4.2).

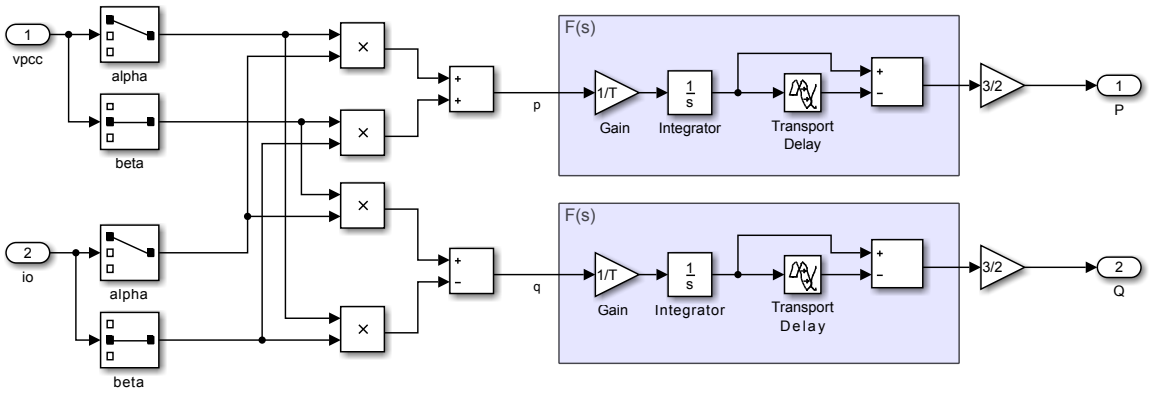

Fig. 4.2 The simulink diagram of power calculator of the Figure. 4.1.

4.2.1 Small-Signal Analysis

A small-signal analysis can be used to investigate the stability of the primary control, considering small disturbance around the stable equilibrium point defined by $(\delta_e, V_{pcce}, E_e)$, where V_{pcce} is the amplitude (RMS) of the voltage at PCC, E_e is the amplitude (RMS) of the VSI's capacitor voltage and δ_e is the phase angle difference between them. Figure. 4.3 shows the three-phase inverter which is modeled as an ideal single-phase voltage source in series with the output impedance $Z_o\underline{/\theta}$. The real and reactive power flowing from the source to the terminal v_{pcc} through the impedance $Z_o\underline{/\theta}$ are as follows[10]:

$$P = \left(\frac{EV_{pcc}}{Z_o}\cos\delta - \frac{V_{pcc}^2}{Z_o}\right)\cos\theta + \frac{EV_{pcc}}{Z_o}\sin\delta\sin\theta \tag{4.12}$$

$$Q = \left(\frac{EV_{pcc}}{Z_o}\cos\delta - \frac{V_{pcc}^2}{Z_o}\right)\sin\theta - \frac{EV_{pcc}}{Z_o}\sin\delta\cos\theta \tag{4.13}$$

The above equations and the ameliorated universal droop controller (4.1-4.2) can be linearized around the equilibrium as:

$$\Delta P(s) = k_{pe}\Delta E(s) + k_{p\delta}\Delta\delta(s) \tag{4.14}$$

$$\Delta Q(s) = k_{qe}\Delta E(s) - k_{q\delta}\Delta\delta(s) \tag{4.15}$$

$$s\Delta E(s) = -n\Delta P_{mes}(s)\alpha_1 - n_d s\Delta P_{mes}(s)\alpha_1 \tag{4.16}$$

$$\Delta\omega(s) = m\Delta Q_{mes}(s)\alpha_2 + m_d s\Delta Q_{mes}(s)\alpha_2 \tag{4.17}$$

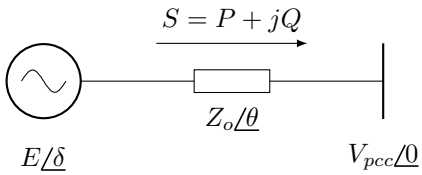

Fig. 4.3 Simplified model of the three-phase VSI.

where:

$$\alpha_1 = \overline{g}_c + g_c n_g \tag{4.18}$$

$$\alpha_2 = \overline{g}_c + g_c m_g \tag{4.19}$$

$$k_{pe} = \frac{V_{pcce}\left(\cos\delta_e \cos\theta + \sin\delta_e \sin\theta\right)}{Z_o} \tag{4.20}$$

$$k_{p\delta} = \frac{E_e V_{pcce}\left(\cos\delta_e \sin\theta - \sin\delta_e \cos\theta\right)}{Z_o} \tag{4.21}$$

$$k_{qe} = \frac{V_{pcce}\left(\cos\delta_e \sin\theta - \sin\delta_e \cos\theta\right)}{Z_o} \tag{4.22}$$

$$k_{q\delta} = \frac{E_e V_{pcce}\left(\sin\delta_e \sin\theta + \cos\delta_e \cos\theta\right)}{Z_o} \tag{4.23}$$

For small-signal analysis, the integration filter (4.11) used to calculate the real and reactive power is approximated using the well known second order Padé approximation and is expressed as follows [3]:

$$F\left(s\right) \approx \frac{1}{\frac{T^2}{12}s^2 + \frac{T}{2}s + 1} \tag{4.24}$$

The measured active and reactive power becomes:

$$\Delta P_{mes}\left(s\right) = \frac{1}{\frac{T^2}{12}s^2 + \frac{T}{2}s + 1}\Delta P\left(s\right) \tag{4.25}$$

$$\Delta Q_{mes}\left(s\right) = \frac{1}{\frac{T^2}{12}s^2 + \frac{T}{2}s + 1}\Delta Q\left(s\right) \tag{4.26}$$

Substituting (4.14-4.25) into (4.16) gives :

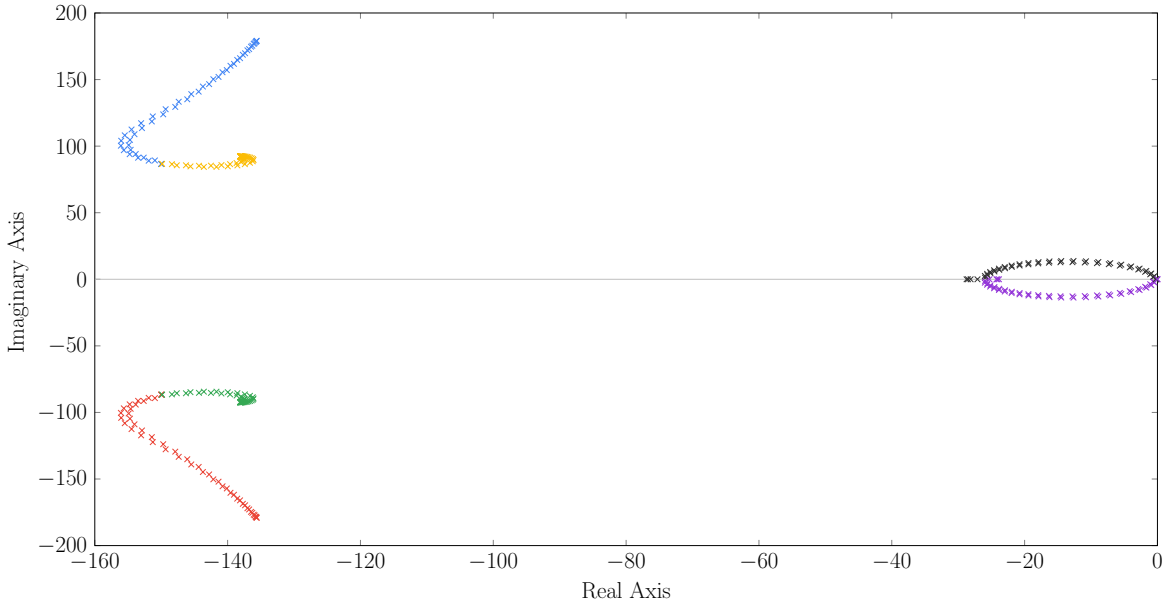

(a)

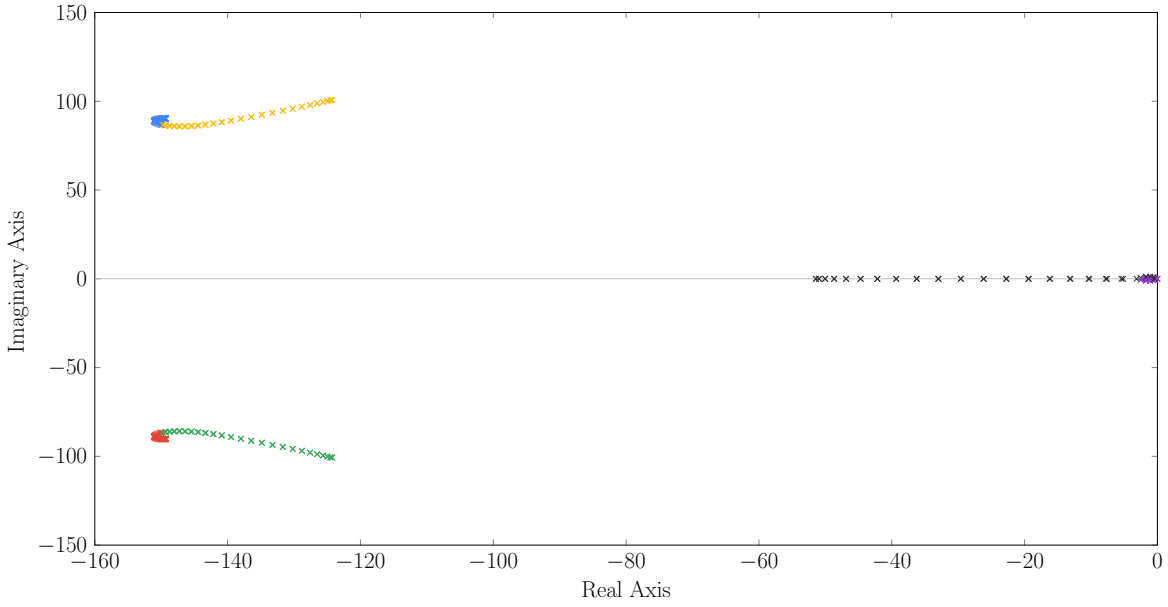

(b)

Fig. 4.4 Root locus plot of the closed-loop system (4.30) when the phase angle of output impedance change from $-\frac{\pi}{2}$ to $\frac{\pi}{2}$ with a resistive inductive load. a) islanded mode ($g_c = 0$) b) grid-connected mode ($g_c = 1$)

$$s\Delta E(s) = -\alpha_1 \frac{n_d s + n}{\frac{T^2}{12}s^2 + \frac{T}{2}s + 1}\left(k_{pe}\Delta E(s) + k_{p\delta}\Delta\delta(s)\right) \tag{4.27}$$

and (4.15-4.26) into (4.17) gives :

$$\Delta\omega(s) = \alpha_2 \frac{m_d s + m}{\frac{T^2}{12}s^2 + \frac{T}{2}s + 1}\left(k_{qe}\Delta E(s) - k_{q\delta}\Delta\delta(s)\right) \tag{4.28}$$

Since :

$$\Delta\omega(s) = s\Delta\delta(s) \tag{4.29}$$

It implies to the following sixth-order homogeneous equation:

$$\begin{aligned} a_6 s^6\Delta\delta(s) + a_5 s^5\Delta\delta(s) + a_4 s^4\Delta\delta(s) + a_3 s^3\Delta\delta(s) + \\ a_2 s^2\Delta\delta(s) + a_1 s\Delta\delta(s) + a_0\Delta\delta(s) = 0 \end{aligned} \tag{4.30}$$

with :

$$a_6 = a^2$$

$$a_5 = 2ab$$

$$a_4 = aC + b^2 + a + \alpha_2 m_d k_{qd} a$$

$$a_3 = aD + bC + b + \alpha_2 m k_{qd} a + \alpha_2 m_d k_{qd} b$$

$$a_2 = bD + C + \alpha_2 m k_{qd} b + \alpha_2 m_d\left(Ck_{qd} + k_{qe}\alpha_1 n_d k_{pd}\right)$$

$$a_1 = D + \alpha_2 m\left(Ck_{qd} + k_{qe}\alpha_1 n_d k_{pd}\right) + \alpha_2 m_d\left(Dk_{qd} + k_{qe}\alpha_1 n k_{pd}\right)$$

$$a_0 = \alpha_2 m\left(Dk_{qd} + k_{qe}\alpha_1 n k_{pd}\right)$$

$$a = T^2/12$$

$$b = T/2$$

$$C = 1 + \alpha_1 n_d k_{pe}$$

$$D = \alpha_1 n k_{pe}$$

The equation (4.30) describes the small-signal dynamics of the closed-loop system around the equilibrium point $(\delta_e, V_{pcce}, E_e)$. Thus, the system stability can be analyzed by the fol-

Table 4.1 The primary control parameters

Inverter	Parameters						
	k_e	n	m	n_d	m_d	n_g	m_g
VSI_1	7	0.2178	3.1×10^{-4}	0.0030	2.0×10^{-6}	0.03	2
VSI_2	7	0.1089	1.6×10^{-4}	0.0015	1.0×10^{-6}	0.03	2
VSI_3	7	0.0726	1.0×10^{-4}	0.0010	6.6×10^{-7}	0.03	2

lowing characteristic equation:

$$a_6 s^6 + a_5 s^5 + a_4 s^4 + a_3 s^3 + a_2 s^2 + a_1 s + a_0 = 0 \tag{4.31}$$

The eigenvalues of this equation (4.31) have been studied for both operation modes when θ of output impedance changes from $-\frac{\pi}{2}$ to $\frac{\pi}{2}$ with $R_o = 0.7\Omega$ ($Z_o = R_o + jR_o \tan(\theta)$), the terminal load $Z_l = 17 + j28$ and the primary control parameters are presented in Table 4.2 (we used the VSI_1 values). E_e and δ_e can be calculated according to output impedance, load impedance and V_{pcce}. Figure. 4.4 shows that all eigenvalues of both modes are in the left half plane which means that regardless to output impedance of VSI the system is always stable during both operation mode, and for this reason we choose the universal droop control.

4.3 Secondary control

However, these decentralized droop controllers cause a deviation of bus voltage amplitude and steady-state frequency from their nominal values. Hence, an upper level of the hierarchy is needed and is called the secondary control. In general, the objective of secondary control in islanded mode is to compensate the mentioned deviations in both steady-state frequency and voltage amplitude. In other hand, during grid-connected mode its role is to smooth the exported power from/to the main grid. Moreover, this level is responsible for synchronization between the islanded microgrid and the main grid in order to ensure a seamless transition.

The secondary control is used to compensate the deviations in amplitude and frequency of the PCC voltage caused by the primary control and restores them to their nominal values.

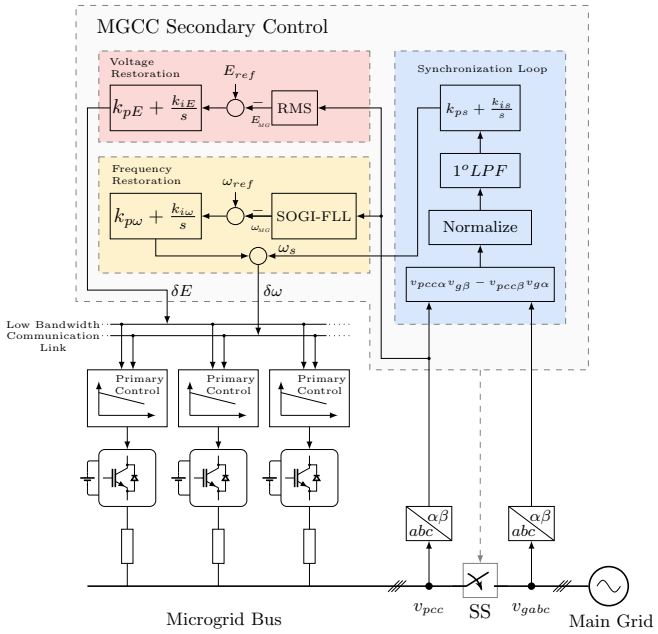

Fig. 4.5 Block diagram of the secondary control in $\alpha\beta$-coordination for voltage restoration, frequency restoration and grid synchronization.

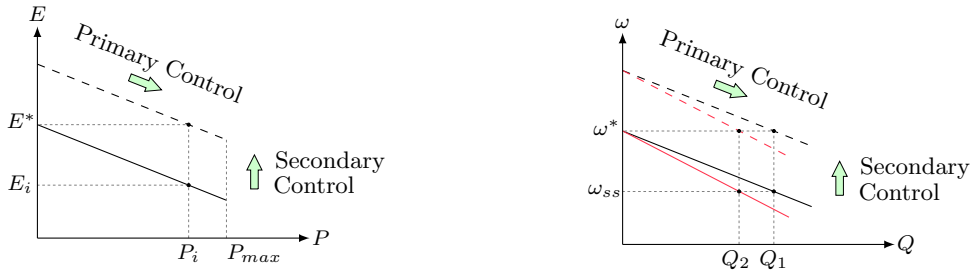

Fig. 4.6 $P-E$ and $Q-\omega$ of primary and secondary control principles.

The restoration controllers can be presented as follows:

$$\delta\omega = k_{p\omega}\left(\omega_{ref} - \omega_{MG}\right) + k_{i\omega}\int\left(\omega_{ref} - \omega_{MG}\right)dt \tag{4.32}$$

$$\delta E = k_{pE}\left(E_{ref} - E_{MG}\right) + k_{iE}\int\left(E_{ref} - E_{MG}\right)dt \tag{4.33}$$

where $k_{p\omega}$, $k_{i\omega}$, k_{pE} and k_{iE} are the PI controllers parameters. $\delta\omega$ and δE are sent to all primary controllers as shown in Figure. 4.5. The Figure. 4.6 shows the principle of this technique that lays on uniform shifting of all primary controllers by an amount of $\delta\omega$ and δE. As

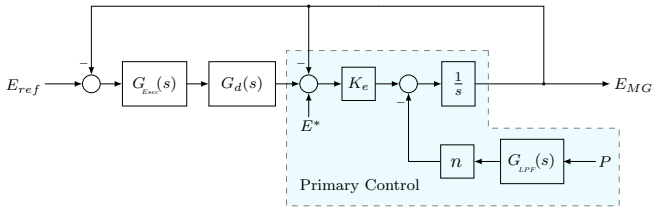

Fig. 4.7 Block diagram of the voltage restoration control.

we use the hierarchical control, the dynamics response of the secondary control is slower than the primary control which allow us to design the controllers separately, and in order to don't exceed the tolerable frequency and amplitude, the secondary controller must be bounded.

4.3.1 Voltage Restoration

Figure. 4.7 shows the model of the voltage restoration control that consists of primary controller, PI controller cascaded with a delay caused by the low bandwidth communication lines G_d. This model is used to analyze the stability of the system and to design the PI controller. Based on the block diagram, the model as follow:

$$E_{MG}(s) = \frac{K_e G_{Esec}(s) G_d(s)}{s + K_e G_{Esec}(s) G_d(s) + K_e} E_{ref}(s) - \frac{n G_{LPF}(s)}{s + K_e G_{Esec}(s) G_d(s) + K_e} P(s) \tag{4.34}$$

Where the transfer functions are given as:

$$G_{Esec}(s) = k_{pE} + \frac{k_{iE}}{s} \tag{4.35}$$

$$G_d(s) = \frac{1}{0.24 \cdot s + 1} \tag{4.36}$$

$$G_{LPF}(s) = \frac{\omega_f}{s + \omega_f} \tag{4.37}$$

The details of the PI controller design is given in next section.

4.3.2 Frequency Restoration

The frequency restoration control has been modeled and analyzed using the same procedure as the voltage restoration control. In Figure. 4.8, $G_{\omega sec}$ is a PI controller, and G_{FLL} is simplified first-order transfer function of SOGI-FLL [78] that used to estimate the frequency of the microgrid voltage at PCC.

4.3.3 Synchronization Loop for Seamless Transition

During the islanded mode, the microgrid may need to connect to the main grid in order to import power in the case where the local demand is not supplied by the paralleled VSIs, or to export the exceed power. We consider that the amplitude and the frequency of the PCC voltage is restored to their nominal values which are assumed to be equal to the nominals of the grid. However, this is not enough to make a smooth transition, because the phase angles are different. Thus, a sudden transition without planning would cause a large circulating current flow from the grid to the VSIs. In order to avoid this issue, the microgrid voltage must be synchronized to the grid voltage before turning ON the SS and starting the grid-connecting mode.

The synchronization process mitigates the phase angle between the two voltages by sending an amount of frequency ω_s to each VSI as shown in Figure. 4.5 through the secondary control.

By using the $\alpha - \beta$ components of the two voltages, we can calculate the grid error as:

$$\varepsilon = v_{pcc\alpha} v_{g\beta} - v_{pcc\beta} v_{g\alpha} \tag{4.38}$$

This error gives a useful index of the synchronization process, which consists of orthogonal product. For simplicity, we assume that v_{pcc} and v_g are purely sinusoidal, then ε becomes:

$$\varepsilon = E^{*2} \sin\left(\phi_G - \phi_{MG}\right) \tag{4.39}$$

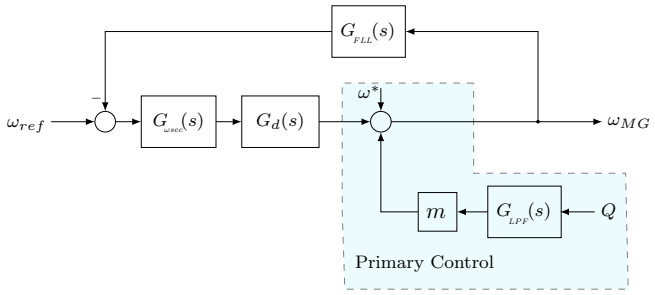

Fig. 4.8 Block diagram of the frequency restoration control.

Where E^* is the voltage amplitude of the grid and the microgrid after restoration, ϕ_{MG} and ϕ_G are the phase angles. After normalizing (4.39), ε equals to:

$$\varepsilon = \sin\left(\phi_G - \phi_{MG}\right) \tag{4.40}$$

Then, for small values of $(\phi_G - \phi_{MG})$, ε becomes:

$$\varepsilon = \phi_G - \phi_{MG} \tag{4.41}$$

Therefore, ε can be fed to a simple PI controller. The synchronization control can be expressed as:

$$\omega_s = \left(v_{pcc\alpha} v_{g\beta} - v_{pcc\beta} v_{g\alpha}\right) \frac{\omega_f}{s + \omega_f} \frac{k_{ps} s + k_{is}}{s} \tag{4.42}$$

Where w_f is a cut-off frequency which is fixed over one decade below the fundamental frequency, k_{ps} and k_{is} are the PI coefficients.

4.4 Optimal Controller Design

In this thesis, the controller parameters of each control level of the hierarchical structure are designed by solving an optimization problem in order to find their optimal values. The optimization problem is defined as minimization of a fitness function that its optimization vector is the controller parameters. The concept stands on evaluating the fitness function after each adjustment of the optimization vector until we find its smallest possible value,

which we assume that corresponds to the optimal controller parameters. Therefore, the key points of this method are the fitness function and the solver that adjust the optimization vector intelligently.

For PR controllers of the inner control, the optimization problem is defined as follows:

$$\begin{aligned} \underset{\theta}{\text{minimize}} \quad & \sum_{t=0}^{\infty} \left(v_{refa}^{t} - v_{Ca}^{t}\left(\theta\right)\right)^{2} + \left(v_{refb}^{t} - v_{Cb}^{t}\left(\theta\right)\right)^{2} + \left(v_{refc}^{t} - v_{Cc}^{t}\left(\theta\right)\right)^{2} \\ \text{subject to} \quad & 0 < \theta_i \leq \theta_{imax},\ i = 1, \ldots, 11. \end{aligned} \tag{4.43}$$

where we choose the integral of squared-error (ISE) as a fitness function since it give us a good index on the signal quality of the capacitor voltage v_{Cabc}, θ is the optimization vector which is the parameters of PR controllers and equals
$\theta = \left[k_{pi}\ k_{ri}\ k_{3i}\ k_{5i}\ k_{7i}\ k_{pv}\ k_{rv}\ k_{3v}\ k_{5v}\ k_{7v}\ \omega_c\right]^T$ and θ_{max} is the upper bound of the parameters which is determined by analyzing the stability of the model (3.3) and (3.4).

For primary controller and PI controllers of secondary level, we have developed a new fitness function in time domain inspired from the integral of time weight absolute-error (ITAE) [92] in order to increase the robust performance and to cope the oscillation.

$$\begin{aligned} \underset{\theta}{\text{minimize}} \quad & \sum_{t=0}^{\infty} t\left|e_t\left(\theta\right)\right|\left[1 + k - k\,\text{sign}\left(e_t\left(\theta\right) + OS \cdot y_d\right)\right] \\ \text{subject to} \quad & 0 < \theta_i \leq \theta_{imax},\ i = 1, \ldots, N. \end{aligned} \tag{4.44}$$

where $e_t\left(\theta\right)$ is the error between desired and actual value by using θ values for the controller parameters at the sampled time t ($e_t\left(\theta\right) = y_d - y_t\left(\theta\right)$), OS is the overshoot and k is a constant value used to penalize the oscillations that are upper then $\left(1 + OS\right) \cdot y_d$. The optimization vector of the primary controller is split in two vectors as there are two operation modes, $\theta_1 = \left[k_e\ n_d\ m_d\right]^T$ for simulation in islanded mode and $\theta_2 = \left[n_g\ m_g\right]^T$ for simulation in grid-connected mode with using the optimal θ_1; the droop coefficients n and m are calculated according to desired voltage droop ratio $e_P = \frac{n_i S_i^*}{K_e E^*}$ and frequency boost ratio $e_Q = \frac{m_i S_i^*}{\omega^*}$.

The optimization vector of PI controller is $\theta = \left[k_p \; k_i\right]^T$. It's good to mention that secondary level has many control loops such as voltage restoration, frequency restoration and synchronization loop which each loop is tunned separately.

To solve the optimization problem of (4.43) and (4.44), we apply a meta-heuristic algorithm which is based on PSO (Particle Swarm Optimization) and is called SLPSO (Self-Learning Particle Swarm Optimizer) [53] (see chapter 2).

The optimal parameters of the hierarchical control are presented in the table 4.2, where $k = 50$, $OS = 0$, $e_P = 0.1$ and $e_Q = 10^{-3}$.

Table 4.2 Optimal parameters of the hierarchical control

Inner Control							
Controller	Parameters						
	k_p	k_r	k_3	k_5	k_7	ω_c	
G_i	0.2131	211.62	32.21	101.1	61.74	0.0015	
G_v	0.2027	205.66	25.35	22.14	61.08	0.0015	
Primary Control							
Inverter	Parameters						
	k_e	n	m	n_d	m_d	n_g	m_g
VSI_1	7	0.2178	3.1×10^{-4}	0.003	2.0×10^{-6}	0.03	2
VSI_2	7	0.1089	1.6×10^{-4}	0.0015	1.0×10^{-6}	0.03	2
VSI_3	7	0.0726	1.0×10^{-4}	0.001	6.6×10^{-7}	0.03	2
Secondary Control							
PI	Voltage loop		Frequency loop		Synchronization		
k_p	1.8151		2.2298		4.5		
k_i	4.2968		7.6729		0		

4.5 Simulation Results

In order to test the proposed control strategy, we have adopted the microgrid structure of the Figure. 4.9. It consists of three VSIs operating in parallel and a local nonlinear load which is composed of three-phase uncontrolled rectifier loaded with LC filter and a variable resistor. Each VSI is connected to the common bus through LCL filter and line impedance that represents a physical distance. In another hand, the microgrid is interfaced to the main grid via an intelligent static switch (SS) that allows monitoring the voltages of both sides [28, 69].

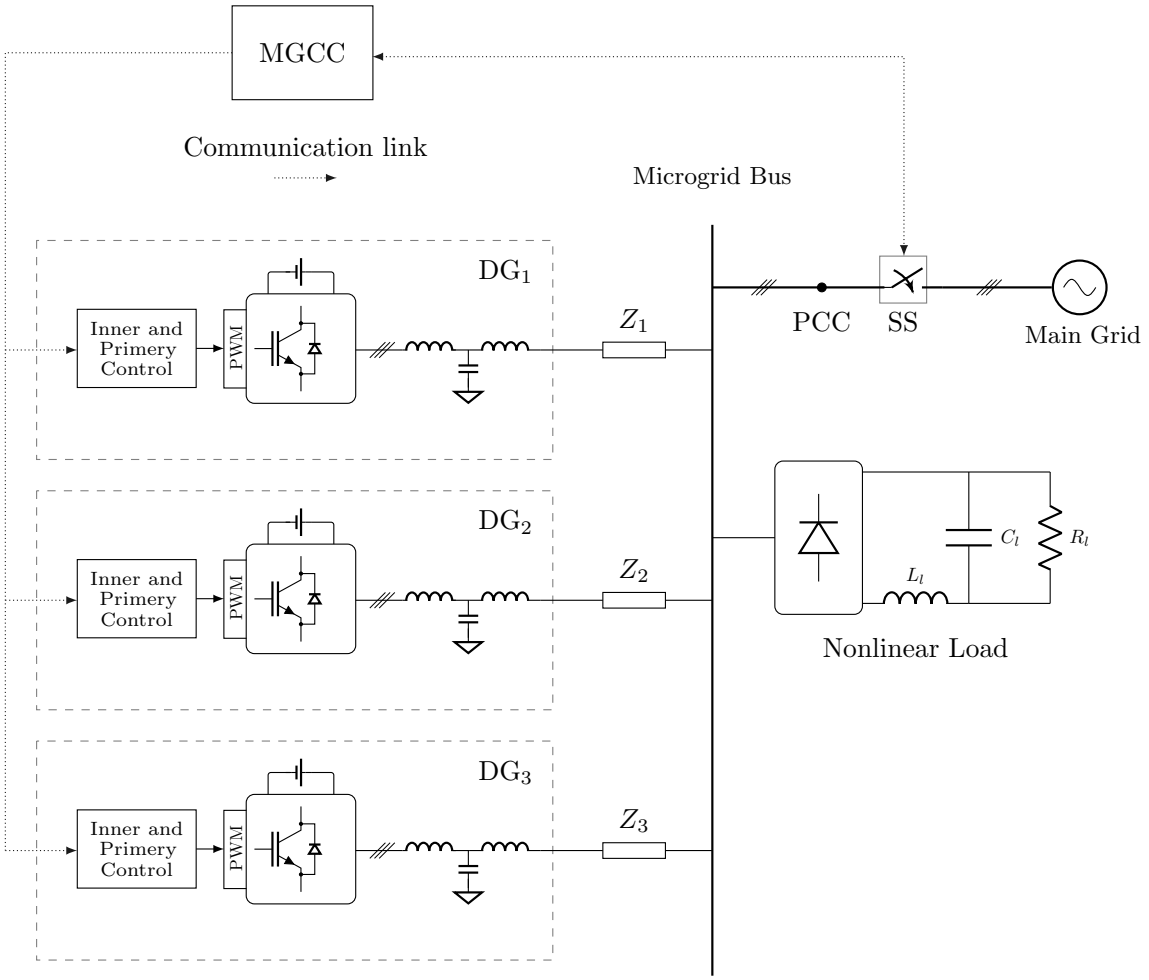

Fig. 4.9 Single line diagram of the microgrid system.

The SS disconnects automatically the microgrid when detects any disturbance or fault in the main grid, and when the grid is restored, SS informs the MGCC to start the synchronization process in order to reconnect.

We evaluate the proposed hierarchical control by simulating the system shown in Figure. 4.9 using MATLAB/Simulink. Three studies with different scenarios are carried out to test the robustness and the performance of the system.

4.5.1 Islanded operation

Initially, a black start was performed to operate the microgrid in islanded mode, where the three inverters start operating in parallel at same time and supplying the nonlinear load.

Table 4.3 Electrical system parameters

Parameter	Symbol	Value	Units
Nominal frequency	ω^*	$2\pi \cdot 50$	rad/s
Nominal RMS voltage	E^*	220	V
Load filter inductance	L_l	84	μH
Load filter capacitance	C_l	500	μC
Load	R_l	300/150/80	Ω

we assume that the load demand still lower than the total power ratings of the inverters during the islanded simulation, which we would like to focus just on the power sharing and the voltage restoration. Figure. 4.11a and Figure. 4.11b show the active and reactive power of the inverters and the nonlinear load while the primary control is running. These figures show clearly that the inverters share both active and reactive power accurately in a ratio of $1 : 2 : 3$. To test the robustness of power sharing of the primary control, we suddenly disconnect the third inverter at $t = 15$, and letting just two inverters supplying the power demand of the nonlinear load. As we see in the Figure. 4.11, the both inverters are handling well the load with time respond of $0.3s$, but if we give a closer look at the load's active power (or reactive power) within the time range of $14s$ to $16s$, we observe that its power is dropped from $930W$ to $880W$ after disconnection of the third inverter. This due to the amplitude of PCC voltage which drops from $220V$ to $216V$ (see Figure. 4.10a) and to its quality where the THD increases from 2.1% to 2.8% as presented in Figure. 4.12 but this still below 5% as recommended by [1]. At $t = 30$, the load demand is increased to double, and regardless of that the inverters still sharing the power with the ratio of 1:2. However, this sharing process which is based on the primary control causes a deviation in amplitude and frequency of the PCC voltage when a disturbance occurs as shown in Figure. 4.10a and Figure. 4.10b. After each static deviation within $3s$, the secondary control starts to restore the amplitude and the frequency to the nominal values, and after that, it will deactivate and letting just the primary control acting. It appears in Figure. 4.11a, that the secondary control affects on the active and reactive power of the load which in turn affects the power delivered by the inverters, and this is evident as the secondary control increases the amplitude of PCC voltage from $212V$ to $220V$ RMS at $t = 34s$.

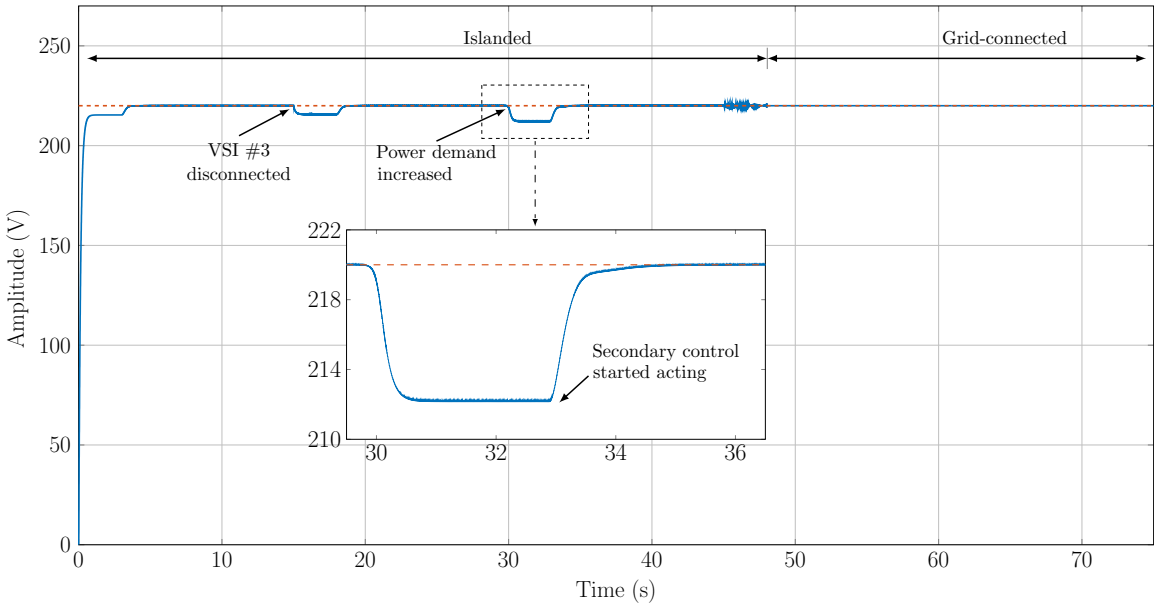

(a)

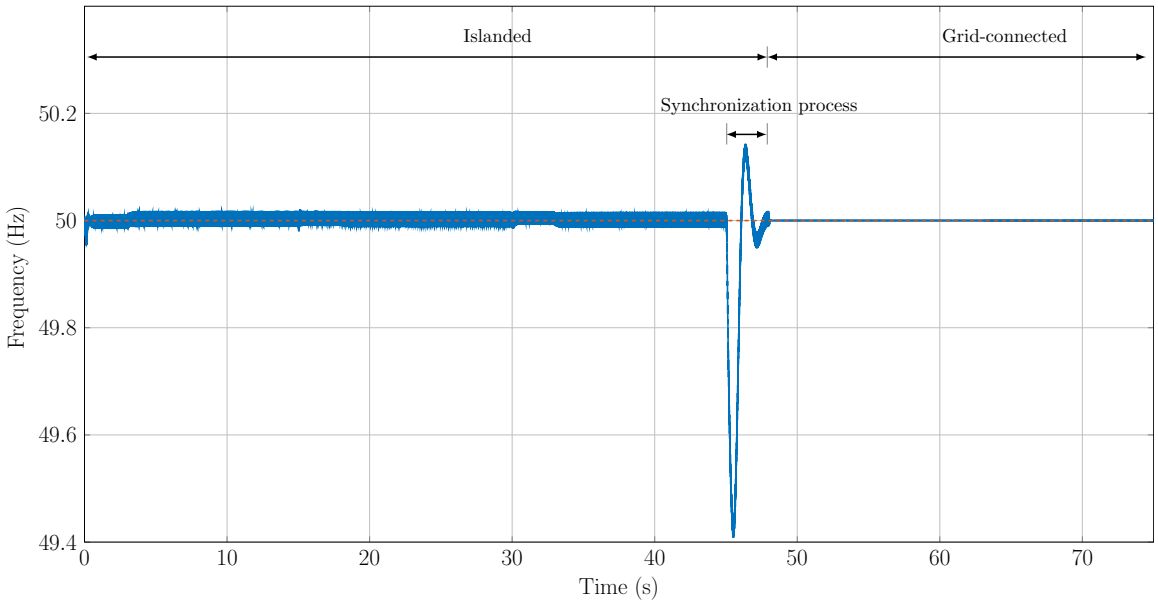

(b)

Fig. 4.10 PCC voltage for a black start of the islanded mode. a) amplitude (RMS) b) frequency.

4.5.2 Transition from islanded to grid-connected mode

For a seamless transition to grid-connected mode, the synchronization control is activated at $t = 45s$. Figure 4.13 shows the phase-a voltage waveform of the microgrid and the grid before and after the synchronization process, it can be observed that within $3s$ the both volt-

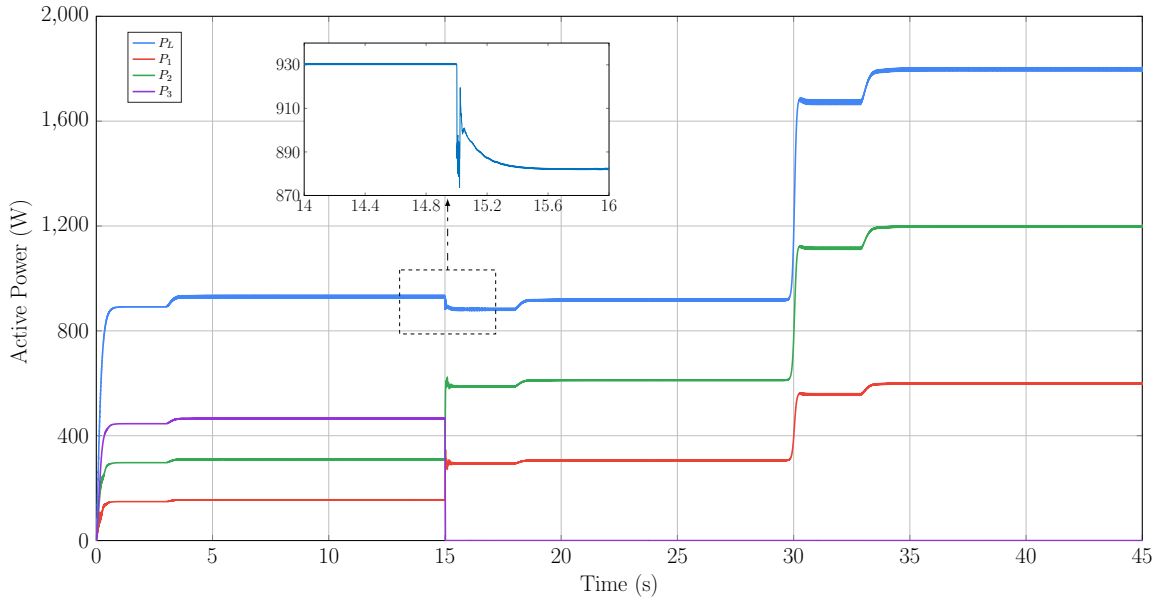

(a)

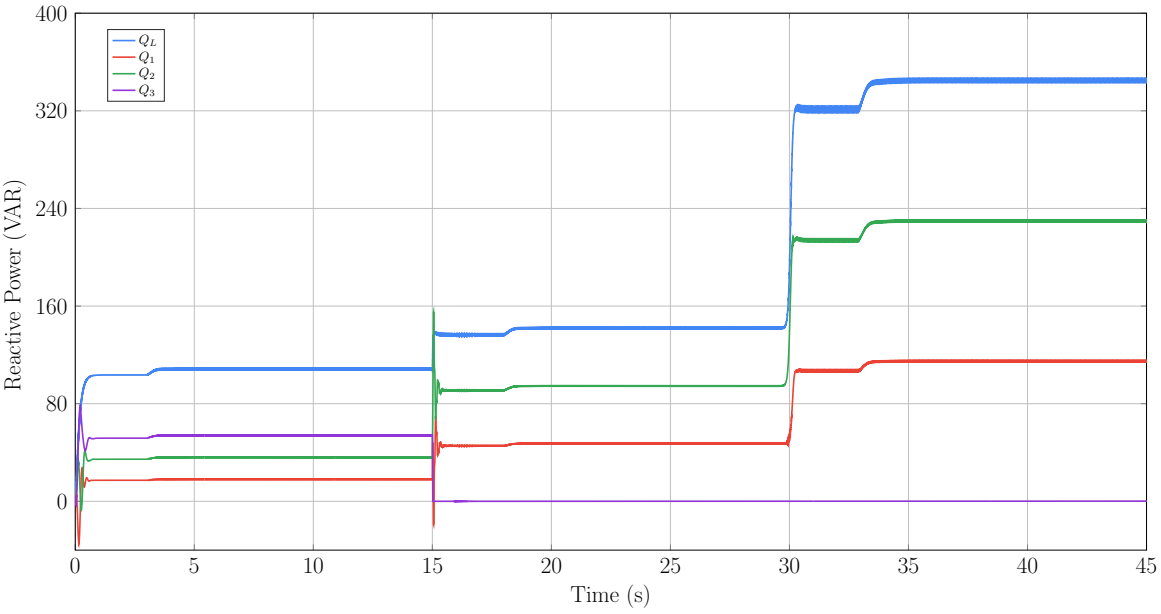

(b)

Fig. 4.11 Power sharing during the islanded mode. a) active power b) reactive power.

ages are synchronized. The phase error between them is shown in Figure. 4.14, where it starts from around 53^o and is still decreasing until arrives to around 0^o at $48s$. However, this process is realized by adjusting the voltage frequency of the microgrid, and this may lead to instability in real world if the frequency exceeds the allowable limit. Thus, there is a trade-

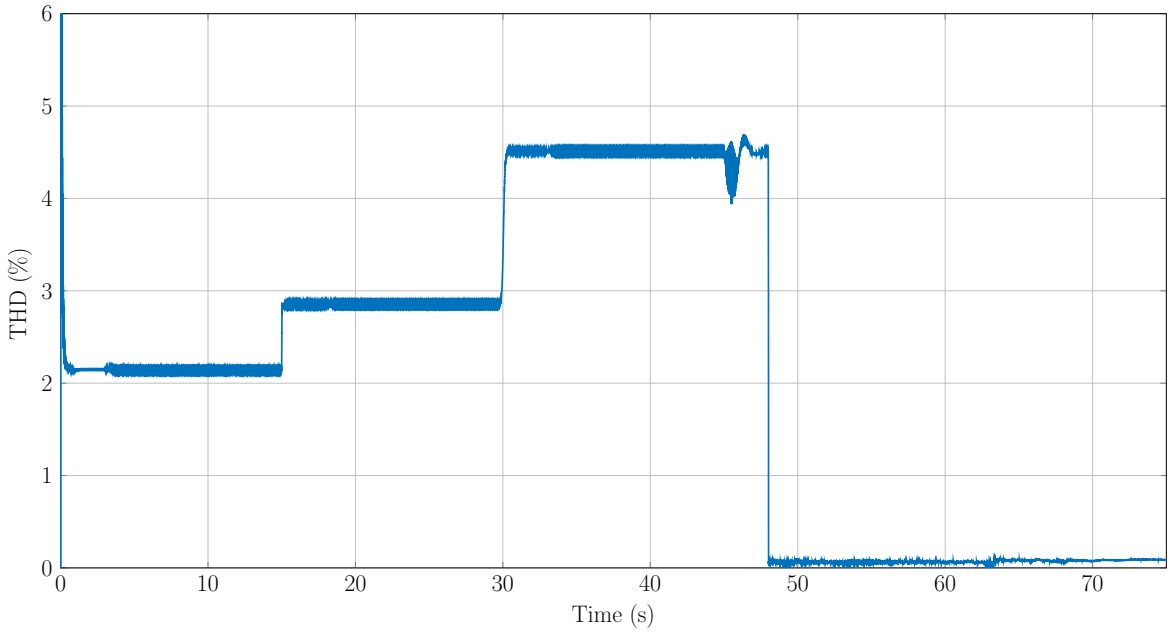

Fig. 4.12 The THD of the microgrid PCC voltage.

off between the time respond of the synchronization process and the maximum deviation of the frequency caused by this process. In Figure. 4.10b, the maximum deviation is about $0.6Hz$ which is tolerable according to Nordel's (North of Europe) grid exigencies. As seen in Figure. 4.10a, the synchronization does not affect on the amplitude of PCC voltage, and this is obvious since the synchronizer compromise just the frequency of each inverter with same amount ω_s. At $t = 48s$, the SS is closed and the microgrid starts the grid-connected mode. The synchronization control is then deactivated.

4.5.3 Grid-connected operation

Once the microgrid is operated in grid-connected mode, the inverters change their behavior from stabilizing the PCC voltage to injecting the scheduled active and reactive power by setting the P^* and Q^* of the primary control. In order to inject the maximum active power from each inverter, the power factor must be set to zero with $P_1^* = 1000W$ and $P_2^* = 2000W$ (the third invert is still disconnected). The reactive demand of the nonlinear load is carried out by the main grid. Hence, the inverters together deliver $3000W$ and the load consumes about $1920W$ as shown in Figure. 4.15a. The excess power is exported to the grid as pre-

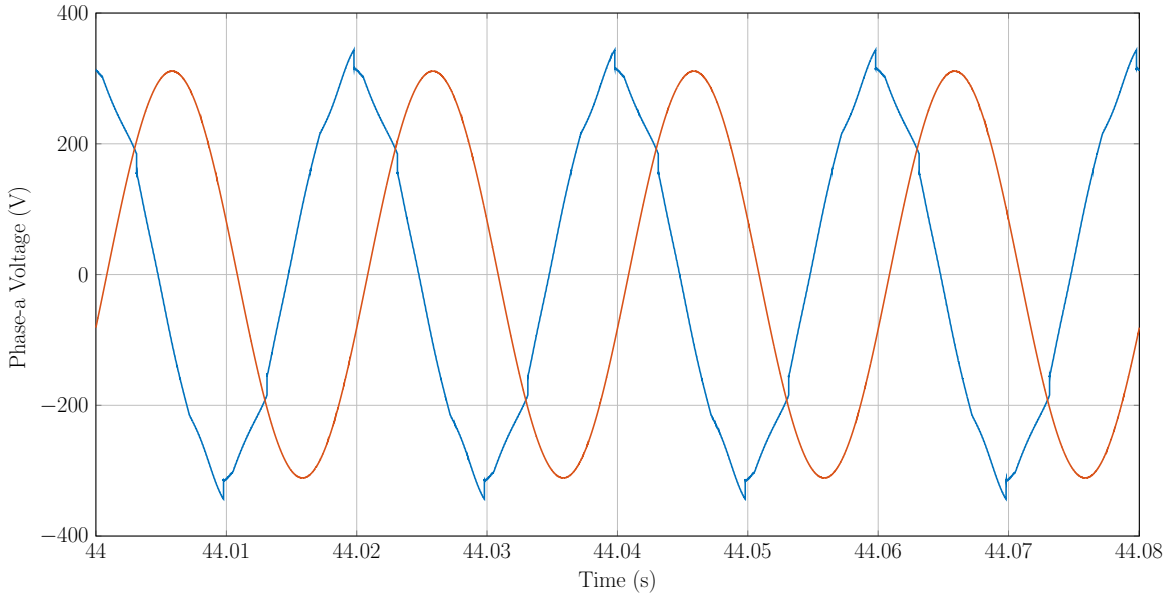

(a)

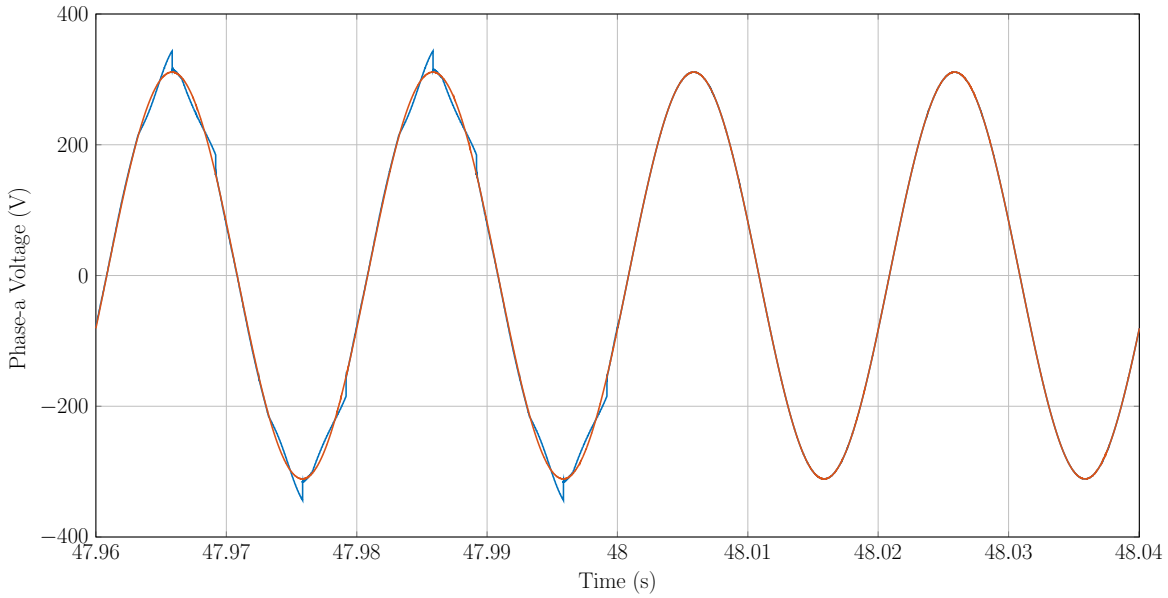

(b)

Fig. 4.13 Synchronization of the microgrid voltage to the grid voltage. a) phase-a voltage waveforms of microgrid and grid before the synchronization process b) after $3s$ of acting, the microgrid starts the grid-connected mode at $t = 48s$.

sented in Figure. 4.15a where the grid's active power is negative ($P_g = -1080W$). At $t = 60s$ the demand is increased to $3565W$ which is greater than the power delivered by the both inverters. Therefore, the microgrid imports the missed power from the grid to satisfy and

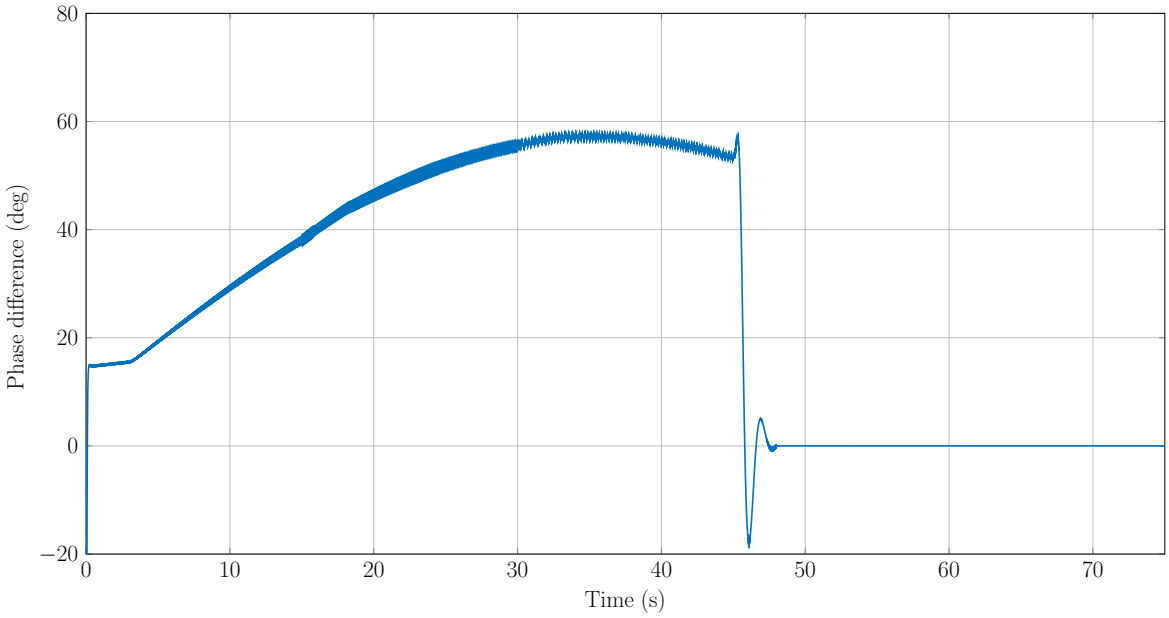

Fig. 4.14 The phase difference between the PCC voltage and the grid voltage.

balance the demand and this demonstrates the bidirectional power flow between the grid and the microgrid.

4.6 Conclusion

In this chapter, a primary control based on the universal droop control has beep proposed. It handles the both modes of operation. When the microgrid operates in islanded mode, the primary control shares the active and reactive power demand among the paralleled VSIs with regardless of their output impedances and when it operates in grid-connected mode, each VSI inject its scheduled power. The secondary control restores the amplitude and the frequency of the PCC voltage caused by the primary control in order to stabilize the microgrid during the islanded mode, and it is responsible for synchronizing the PCC voltage with the grid voltage to make a smooth transition to the grid-connected mode. The model of different control level has been developed to analyze the system stability and to aid to design their controller parameters. Moreover, these parameters have been tuned optimally by solving an optimization problem using a meta-heuristic algorithm called SLPSO. The simulation results

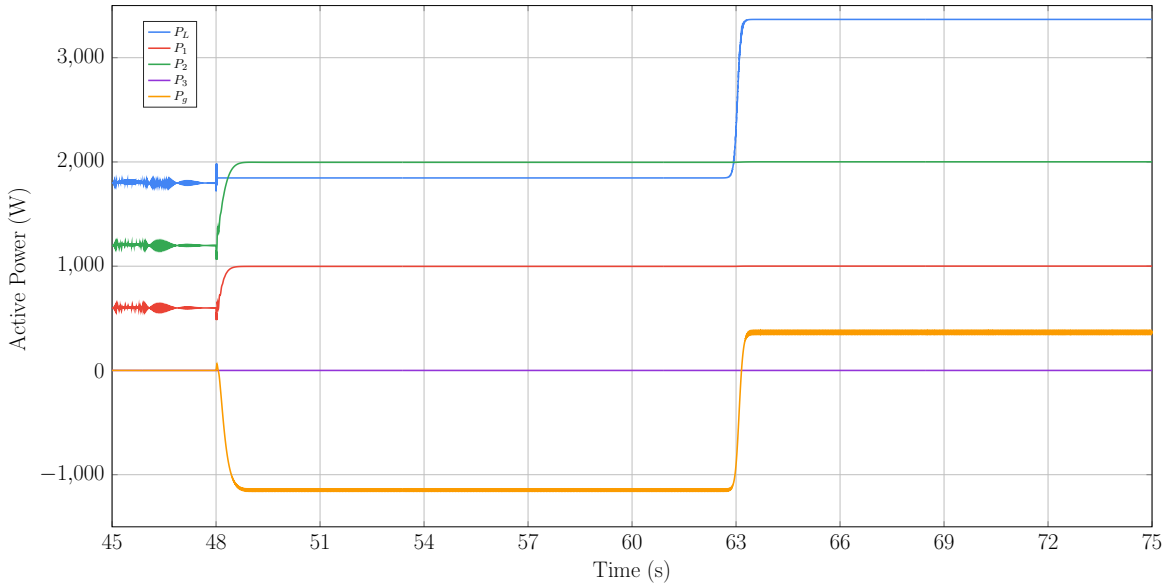

(a)

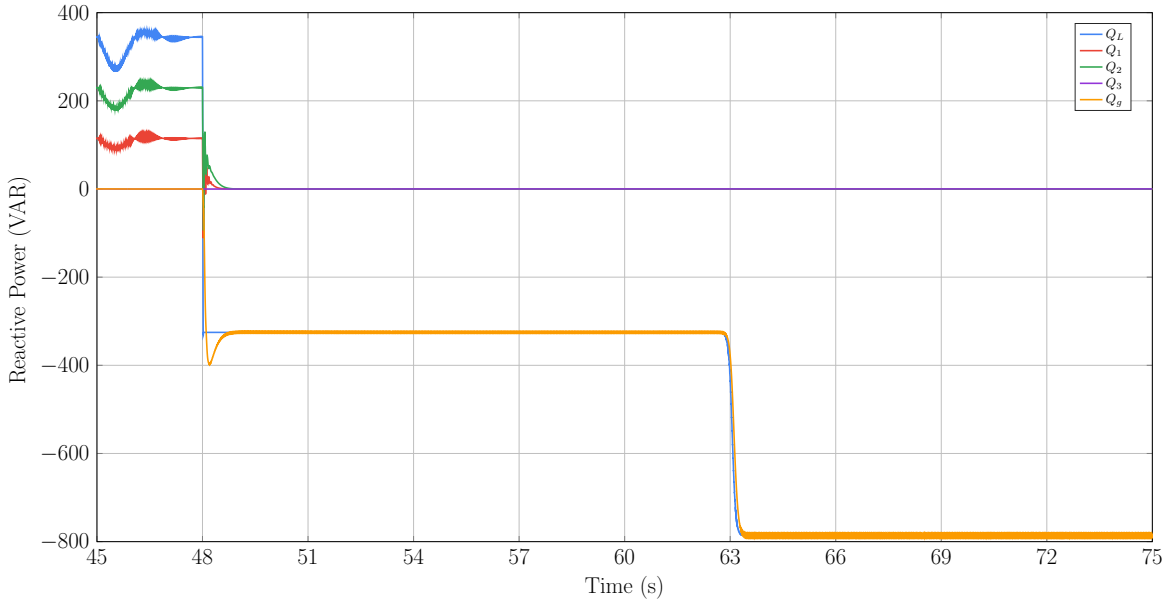

(b)

Fig. 4.15 Active and reactive power of the microgrid during grid-connected mode.

demonstrate the robustness and the performance of the proposed hierarchical control for the flexible microgrid.

Conclusion and future works

The main aim of this thesis was the development of a control method to improve the robustness of an microgrid and to guarantee the stability of distributed generators with a high power quality.

In order to achieve this aim, a control technique has been proposed at the distribution level which is based on hierarchical control framework. This latter, includes inner, primary and secondary control levels. In Chapter 2, a detailed modeling of the distributed generator connected to a LCL filter has been proposed. The proposed power interface uses voltage-current cascade control to maximize disturbance rejection performance within the distributed generator. Moreover, a virtual impedance loop has been used to improve the power quality. A theoretical analysis and a simulation are presented to demonstrate the effectiveness of the proposed control system and the behavior of the controllers in the face of harmonics and disturbance rejection. The proposed strategy significantly improves the THD of voltage.

The conventional droop control method is used for frequency control in power systems. Due to the substantial differences between low voltage microgrids and power systems (R/X report, load characteristics), the conventional droop method is not suitable for low voltage microgrids that are mainly connected to resistive lines.

In Chapter 3, a new technique of droop control based on the universal droop control has been proposed that generates the reference voltage of the inner control which its principal role is to coordinate the distributed generators in a decentralized manner to share the active and the reactive power demand among them. The proposed new primary control technique provides an improved dynamic performance of the microgrid and minimized active/reactive

power sharing errors with inductive and resistive line impedances, as well as provides high reliability and robustness during grid-connected mode.

The secondary control restores the amplitude and the frequency of the PCC voltage caused by the primary control in order to stabilize the microgrid during the islanded mode, and it is responsible for synchronizing the PCC voltage with the grid voltage to make a smooth transition to the grid-connected mode. The model of different control level has been developed to analyze the system stability and to aid to design their controller parameters. Moreover, these parameters have been tuned optimally by solving an optimization problem using a meta-heuristic algorithm called SLPSO.

In Chapter 4, the simulation results show the validity and effectiveness of the proposed controller.

4.7 Future works

Some future research opportunities based on the work presented in this thesis are discussed below.

- Without communication, the droop control provides only stable power sharing. However, the desired features in a microgrid, such as monitoring, regulate the relative power-sharing, etc., require a communication mechanism between the distributed generators. Any practical microgrid requires communication to ensure robustness and prevent outages. Thus this work can be extended to introduce a centralized and decentralized energy management system at the secondary control level to distribute power between distributed generators.

- The development of a hierarchical control architecture to maXImIser the export of active and reactive power to the medium voltage distribution grid by coupling the microgrid voltage and guarantee stability in the system.

- Development of a droop control method for microgrids with distributed energy storage systems (DESS) and hybrid PV / battery units, to balance the state of charge (SoC) and

maintain a comparable number of cycles of charge / discharge between the batteries, while preserving the power balance in the microgrid.

References

[1] (2014). IEEE recommended practice and requirements for harmonic control in electric power systems. *IEEE Std 519-2014 (Revision of IEEE Std 519-1992)*, pages 1–29.

[2] Abdel-Rady Ibrahim Mohamed, Y. and El-Saadany, E. F. (2007). An improved deadbeat current control scheme with a novel adaptive self-tuning load model for a three-phase pwm voltage-source inverter. *IEEE Transactions on Industrial Electronics*, 54(2):747–759.

[3] Abusara, M. A., Sharkh, S. M., and Guerrero, J. M. (2015). Improved droop control strategy for grid-connected inverters. *Sustainable Energy, Grids and Networks*, 1:10 – 19.

[4] Ahn, S., Park, J., Chung, I., Moon, S., Kang, S., and Nam, S. (2010). Power-sharing method of multiple distributed generators considering control modes and configurations of a microgrid. *IEEE Transactions on Power Delivery*, 25(3):2007–2016.

[5] Alepuz, S., Salaet, J., Gilabert, A., Bordonau, J., and Peracaula, J. (2003). Optimal regulator with integral action and gain-scheduling for the comprehensive control of three-level npc vsi. In *IEEE 34th Annual Conference on Power Electronics Specialist, 2003. PESC '03.*, volume 3, pages 1420–1425 vol.3.

[6] Arricibita, D., Sanchis, P., González, R., and Marroyo, L. (2017). Impedance emulation for voltage harmonic compensation in pwm stand-alone inverters. *IEEE Transactions on Energy Conversion*, 32(4):1335–1344.

[7] Asbafkan, A., Mirzaeeian, B., Niroomand, M., and Zarchi, H. A. (2013). Frequency adaptive repetitive control of grid connected inverter for wind turbine applications. In *2013 21st Iranian Conference on Electrical Engineering (ICEE)*, pages 1–6.

[8] Baek, Y., Lee, K., and Hyun, D. (2009). Improved predictive current control for grid connected inverter applications with parameter estimation. pages 1–6.

[9] Basso, T. S. and DeBlasio, R. (2004). Ieee 1547 series of standards: interconnection issues. *IEEE Transactions on Power Electronics*, 19(5):1159–1162.

[10] Bergen, A. R. (2000). *Power systems analysis, 2nd edition*. Prentice Hall, Englewood Cliffs (N.J.).

[11] Bo Yang, Jiande Wu, Xiaodong Lu, and Xiangning He (2008). An improved dsp-based control strategy with predictive current control and fuzzy voltage control for grid-connected voltage source inverters. In *2008 34th Annual Conference of IEEE Industrial Electronics*, pages 2296–2300.

[12] Borup, U., Blaabjerg, F., and Enjeti, P. N. (2001). Sharing of nonlinear load in parallel-connected three-phase converters. *IEEE Transactions on Industry Applications*, 37(6):1817–1823.

[13] Chandorkar, M. C., Divan, D. M., and Adapa, R. (1993). Control of parallel connected inverters in standalone ac supply systems. *IEEE Transactions on Industry Applications*, 29(1):136–143.

[14] Chen, D., Zhang, J., and Qian, Z. (2013). An improved repetitive control scheme for grid-connected inverter with frequency-adaptive capability. *Industrial Electronics, IEEE Transactions on*, 60:814–823.

[15] Chen, D., Zhang, J., and Qian, Z. (2013). Research on fast transient and 6n ± 1 harmonics suppressing repetitive control scheme for three-phase grid-connected inverters. *IET Power Electronics*, 6(3):601–610.

[16] Chen, G. and Feng, E. (2015). Distributed secondary control and optimal power sharing in microgrids. *IEEE/CAA Journal of Automatica Sinica*, 2(3):304–312.

[17] Choudar, A., Boukhetala, D., Barkat, S., and Brucker, J.-M. (2015). A local energy management of a hybrid PV-storage based distributed generation for microgrids. *Energy Conversion and Management*, 90:21 – 33.

[18] Clerc, M. (1999). The swarm and the queen: towards a deterministic and adaptive particle swarm optimization. In *Proceedings of the 1999 Congress on Evolutionary Computation-CEC99 (Cat. No. 99TH8406)*, volume 3, pages 1951–1957 Vol. 3.

[19] Dai, X. and Chao, Q. (2009). The research of photovoltaic grid-connected inverter based on adaptive current hysteresis band control scheme. In *2009 International Conference on Sustainable Power Generation and Supply*, pages 1–8.

[20] De Brabandere, K., Bolsens, B., Van den Keybus, J., Woyte, A., Driesen, J., and Belmans, R. (2007). A voltage and frequency droop control method for parallel inverters. *IEEE Transactions on Power Electronics*, 22(4):1107–1115.

[21] Eberhart, R. C. and Xiaohui Hu (1999). Human tremor analysis using particle swarm optimization. In *Proceedings of the 1999 Congress on Evolutionary Computation-CEC99 (Cat. No. 99TH8406)*, volume 3, pages 1927–1930 Vol. 3.

[22] Espi, J. M., Castello, J., García-Gil, R., Garcera, G., and Figueres, E. (2011). An adaptive robust predictive current control for three-phase grid-connected inverters. *IEEE Transactions on Industrial Electronics*, 58(8):3537–3546.

[23] Falahi, M., Butler-Purry, K., and Ehsani, M. (2013). Dynamic reactive power control of islanded microgrids. *IEEE Transactions on Power Systems*, 28(4):3649–3657.

[24] Fusheng, L., Ruisheng, L., and Fengquan, Z. (2016). Chapter 3 - microgrid and distributed generation. In Fusheng, L., Ruisheng, L., and Fengquan, Z., editors, *Microgrid Technology and Engineering Application*, pages 29 – 46. Academic Press, Oxford.

[25] Ghazanfari, A., Hamzeh, M., Mokhtari, H., and Karimi, H. (2012). Active power management of multihybrid fuel cell/supercapacitor power conversion system in a medium voltage microgrid. *IEEE Transactions on Smart Grid*, 3(4):1903–1910.

[26] Guerrero, J. M., de Vicuna, L. G., Matas, J., Castilla, M., and Miret, J. (2004). A wireless controller to enhance dynamic performance of parallel inverters in distributed generation systems. *IEEE Transactions on Power Electronics*, 19(5):1205–1213.

[27] Guerrero, J. M., Luis Garcia de Vicuna, Matas, J., Castilla, M., and Miret, J. (2005). Output impedance design of parallel-connected ups inverters with wireless load-sharing control. *IEEE Transactions on Industrial Electronics*, 52(4):1126–1135.

[28] Guerrero, J. M., Vasquez, J. C., Matas, J., Castilla, M., and de Vicuna, L. G. (2009). Control strategy for flexible microgrid based on parallel line-interactive UPS systems. *IEEE Transactions on Industrial Electronics*, 56(3):726–736.

[29] Guerrero, J. M., Vasquez, J. C., Matas, J., de Vicuna, L. G., and Castilla, M. (2011). Hierarchical control of droop-controlled AC and DC microgrids - general approach toward standardization. *IEEE Transactions on Industrial Electronics*, 58(1):158–172.

[30] Guofei, T., Guochun, X., Zhibo, Z., and Yong, L. (2012). A control method with grid disturbances suppression for a single-phase lcl-filter-based grid-connected inverter. In *2012 Twenty-Seventh Annual IEEE Applied Power Electronics Conference and Exposition (APEC)*, pages 1489–1493.

[31] Hamzeh, M., Mokhtari, H., and Karimi, H. (2013). A decentralized self-adjusting control strategy for reactive power management in an islanded multi-bus mv microgrid. *Canadian Journal of Electrical and Computer Engineering*, 36(1):18–25.

[32] Han, H., Hou, X., Yang, J., Wu, J., Su, M., and Guerrero, J. M. (2016). Review of power sharing control strategies for islanding operation of ac microgrids. *IEEE Transactions on Smart Grid*, 7(1):200–215.

[33] Han, H., Liu, Y., Sun, Y., Su, M., and Guerrero, J. M. (2015). An improved droop control strategy for reactive power sharing in islanded microgrid. *IEEE Transactions on Power Electronics*, 30(6):3133–3141.

[34] Hao, X., Yang, X., Xie, R., Huang, L., Liu, T., and Li, Y. (2013). A fixed switching frequency integral resonant sliding mode controller for three-phase grid-connected photovoltaic inverter with lcl-filter. In *2013 IEEE ECCE Asia Downunder*, pages 793–798.

[35] He, J. and Li, Y. W. (2012). An enhanced microgrid load demand sharing strategy. *IEEE Transactions on Power Electronics*, 27(9):3984–3995.

[36] He, J., Li, Y. W., and Blaabjerg, F. (2013). An accurate autonomous islanding microgrid reactive power, imbalance power and harmonic power sharing scheme. pages 1337–1343.

[37] He, J., Li, Y. W., Guerrero, J. M., Blaabjerg, F., and Vasquez, J. C. (2013). Microgrid reactive and harmonic power sharing using enhanced virtual impedance. In *2013 Twenty-Eighth Annual IEEE Applied Power Electronics Conference and Exposition (APEC)*, pages 447–452.

[38] Heo, H., Choe, G., and Mok, H. (2013). Robust predictive current control of a grid-connected inverter with harmonics compensation. pages 2212–2217.

[39] Hirsch, A., Parag, Y., and Guerrero, J. (2018). Microgrids: A review of technologies, key drivers, and outstanding issues. *Renewable and Sustainable Energy Reviews*, 90:402 – 411.

[40] Holland, J. (1975). Adaptation in natural and artificial systems. *University of Michigan Press*.

[41] Hornik, T. and Zhong, Q.-C. (2009). H∞ repetitive current controller for grid-connected inverters. *IECON Proceedings (Industrial Electronics Conference)*, pages 554 – 559.

[42] Howell, S., Rezgui, Y., Hippolyte, J.-L., Jayan, B., and Li, H. (2017). Towards the next generation of smart grids: Semantic and holonic multi-agent management of distributed energy resources. *Renewable and Sustainable Energy Reviews*, 77:193 – 214.

[43] Hu, J. and Zhu, Z. Q. (2013). Improved voltage-vector sequences on dead-beat predictive direct power control of reversible three-phase grid-connected voltage-source converters. *IEEE Transactions on Power Electronics*, 28(1):254–267.

[44] Jia, Y., Zhao, J., and Fu, X. (2014). Direct grid current control of lcl-filtered grid-connected inverter mitigating grid voltage disturbance. *IEEE Transactions on Power Electronics*, 29(3):1532–1541.

[45] Jiabing Hu and Bin Hu (2010). Direct active and reactive power regulation of grid connected voltage source converters using sliding mode control approach. In *2010 IEEE International Symposium on Industrial Electronics*, pages 3877–3882.

[46] Kahrobaeian, A. and Ibrahim Mohamed, Y. A. (2015). Networked-based hybrid distributed power sharing and control for islanded microgrid systems. *IEEE Transactions on Power Electronics*, 30(2):603–617.

[47] Kekatos, V., Wang, G., Conejo, A. J., and Giannakis, G. B. (2015). Stochastic reactive power management in microgrids with renewables. *IEEE Transactions on Power Systems*, 30(6):3386–3395.

[48] Keles, C., Alagoz, B. B., and Kaygusuz, A. (2015). A note on demand side load management by maximum power limited load shedding algorithm for smart grids. In *2015 3rd International Istanbul Smart Grid Congress and Fair (ICSG)*, pages 1–5.

[49] Kennedy, J. and Eberhart, R. (1995). Particle swarm optimization. In *Proceedings of ICNN'95 - International Conference on Neural Networks*, volume 4, pages 1942–1948 vol.4.

[50] Kim, J.-Y., Park, J. H., and Lee, H.-J. (2011). Coordinated control strategy for microgrid in grid-connected and islanded operation. *IFAC Proceedings Volumes*, 44(1):14766 – 14771. 18th IFAC World Congress.

[51] Kirkpatrick, S., Gelatt, C. D., and Vecchi, M. P. (1983). Optimization by simulated annealing. *Science*, 220(4598):671–680.

[52] Li, C., Yang, S., and Nguyen, T. T. (2012). A self-learning particle swarm optimizer for global optimization problems. *IEEE Transactions on Systems, Man, and Cybernetics, Part B (Cybernetics)*, 42(3):627–646.

[53] Li, C., Yang, S., and Nguyen, T. T. (2012). A self-learning particle swarm optimizer for global optimization problems. *IEEE Transactions on Systems, Man, and Cybernetics, Part B (Cybernetics)*, 42(3):627–646.

[54] Li, Q., Chen, F., Chen, M., Guerrero, J. M., and Abbott, D. (2016). Agent-based decentralized control method for islanded microgrids. *IEEE Transactions on Smart Grid*, 7(2):637–649.

[55] Loh, P., Tang, Y., Blaabjerg, F., and Wang, P. (2011). Mixed-frame and stationary-frame repetitive control schemes for compensating typical load and grid harmonics. *Power Electronics, IET*, 4:218 – 226.

[56] Ma, C. and Huang, D. (2011). Comparative study of pi controller and fuzzy logic controller for three-phase grid-connected inverter. In *2011 IEEE International Conference on Mechatronics and Automation*, pages 2067–2071.

[57] Mahmood, H., Michaelson, D., and Jiang, J. (2015a). Accurate reactive power sharing in an islanded microgrid using adaptive virtual impedances. *IEEE Transactions on Power Electronics*, 30(3):1605–1617.

[58] Mahmood, H., Michaelson, D., and Jiang, J. (2015b). Reactive power sharing in islanded microgrids using adaptive voltage droop control. *IEEE Transactions on Smart Grid*, 6(6):3052–3060.

[59] Malesani, L., Mattavelli, P., and Buso, S. (1998). Robust dead-beat current control for pwm rectifiers and active filters. In *Conference Record of 1998 IEEE Industry Applications Conference. Thirty-Third IAS Annual Meeting (Cat. No.98CH36242)*, volume 2, pages 1377–1384 vol.2.

[60] Malesani, L., Mattavelli, P., and Tomasin, P. (1997). Improved constant-frequency hysteresis current control of vsi inverters with simple feedforward bandwidth prediction. *IEEE Transactions on Industry Applications*, 33(5):1194–1202.

[61] Mao, M., Dong, Z., Ding, Y., and Chang, L. (2014). A unified controller for a microgrid based on adaptive virtual impedance and conductance. In *2014 IEEE Energy Conversion Congress and Exposition (ECCE)*, pages 695–701.

[62] Micallef, A., Apap, M., Spiteri-Staines, C., and Guerrero, J. M. (2012). Cooperative control with virtual selective harmonic capacitance for harmonic voltage compensation in islanded microgrids. In *IECON 2012 - 38th Annual Conference on IEEE Industrial Electronics Society*, pages 5619–5624.

[63] Micallef, A., Apap, M., Spiteri-Staines, C., and Guerrero, J. M. (2013). Selective virtual capacitive impedance loop for harmonic voltage compensation in islanded microgrids. In *IECON 2013 - 39th Annual Conference of the IEEE Industrial Electronics Society*, pages 7968–7973.

[64] Milczarek, A., Malinowski, M., and Guerrero, J. M. (2015). Reactive power management in islanded microgrid—proportional power sharing in hierarchical droop control. *IEEE Transactions on Smart Grid*, 6(4):1631–1638.

[65] Mohamed, Y. A. I. and El-Saadany, E. F. (2008). Adaptive decentralized droop controller to preserve power sharing stability of paralleled inverters in distributed generation microgrids. *IEEE Transactions on Power Electronics*, 23(6):2806–2816.

[66] Mohamed, Y. A. I. and Radwan, A. A. (2011). Hierarchical control system for robust microgrid operation and seamless mode transfer in active distribution systems. *IEEE Transactions on Smart Grid*, 2(2):352–362.

[67] Mohamed, Y. A. I., Zeineldin, H. H., Salama, M. M. A., and Seethapathy, R. (2012). Seamless formation and robust control of distributed generation microgrids via direct voltage control and optimized dynamic power sharing. *IEEE Transactions on Power Electronics*, 27(3):1283–1294.

[68] Nutkani, I. U., Loh, P. C., Wang, P., and Blaabjerg, F. (2016). Linear decentralized power sharing schemes for economic operation of ac microgrids. *IEEE Transactions on Industrial Electronics*, 63(1):225–234.

[69] Olivares, D. E., Mehrizi-Sani, A., Etemadi, A. H., Cañizares, C. A., Iravani, R., Kazerani, M., Hajimiragha, A. H., Gomis-Bellmunt, O., Saeedifard, M., Palma-Behnke, R., Jiménez-Estévez, G. A., and Hatziargyriou, N. D. (2014). Trends in microgrid control. *IEEE Transactions on Smart Grid*, 5(4):1905–1919.

[70] Owusu, P. A. and Asumadu-Sarkodie, S. (2016). A review of renewable energy sources, sustainability issues and climate change mitigation. *Cogent Engineering*, 3(1).

[71] Parhizi, S., Lotfi, H., Khodaei, A., and Bahramirad, S. (2015). State of the art in research on microgrids: A review. *IEEE Access*, 3:890–925.

[72] Peltoniemi, P., Nuutinen, P., Niemela, M., and Pyrhonen, J. (2009). Lqg-based voltage control of the single-phase inverter for noisy environment. In *2009 13th European Conference on Power Electronics and Applications*, pages 1–10.

[73] Peng, F. Z. and Lai, J.-S. (1996). Generalized instantaneous reactive power theory for three-phase power systems. *IEEE Transactions on Instrumentation and Measurement*, 45(1):293–297.

[74] Qing-Chang Zhong, Green, T., Jun Liang, and Weiss, G. (2002). Robust repetitive control of grid-connected dc-ac converters. 3:2468–2473 vol.3.

[75] Revuelta, P. S., Litrán, S. P., and Thomas, J. P. (2016). 8 - distributed generation. In Revuelta, P. S., Litrán, S. P., and Thomas, J. P., editors, *Active Power Line Conditioners*, pages 285 – 322. Academic Press, San Diego.

[76] Reynolds, J., Ahmad, M. W., Rezgui, Y., and Hippolyte, J.-L. (2019). Operational supply and demand optimisation of a multi-vector district energy system using artificial neural networks and a genetic algorithm. *Applied Energy*, 235:699 – 713.

[77] Richard C. Dorf, R. H. B. (2016). *Modern Control Systems, 13th Edition*. Pearson.

[78] Rodríguez, P., Luna, A., Muñoz-Aguilar, R. S., Etxeberria-Otadui, I., Teodorescu, R., and Blaabjerg, F. (2012). A stationary reference frame grid synchronization system for three-phase grid-connected power converters under adverse grid conditions. *IEEE Transactions on Power Electronics*, 27(1):99–112.

[79] Sachs, T., Gründler, A., Rusic, M., and Fridgen, G. (2019). Framing microgrid design from a business and information systems engineering perspective. *Business & Information Systems Engineering*.

[80] Sad Abadi, M. S. (2016). Fixed-structure control of lti systems with polytopic-type uncertainty application to inverter-interfaced microgrids. page 197.

[81] Sajadi, A., Strezoski, L., Strezoski, V., Prica, M., and Loparo, K. A. (2019). Integration of renewable energy systems and challenges for dynamics, control, and automation of electrical power systems. *Wiley Interdisciplinary Reviews: Energy and Environment*, 8(1):e321.

[82] Savaghebi, M., Jalilian, A., Vasquez, J. C., and Guerrero, J. M. (2013). Autonomous voltage unbalance compensation in an islanded droop-controlled microgrid. *IEEE Transactions on Industrial Electronics*, 60(4):1390–1402.

[83] Savaghebi, M., Shafiee, Q., Vasquez, J. C., and Guerrero, J. M. (2015). Adaptive virtual impedance scheme for selective compensation of voltage unbalance and harmonics in microgrids. In *2015 IEEE Power Energy Society General Meeting*, pages 1–5.

[84] Shah, T. and Ansari, Z. A. (2018). An overview of intelligent energy management system for dc microgrid: System and communication architecture and application in power distribution system. pages 1–4.

[85] Shang, L., Sun, D., and Hu, J. (2011). Sliding-mode-based direct power control of grid-connected voltage-sourced inverters under unbalanced network conditions. *IET Power Electronics*, 4(5):570–579.

[86] Shi, D., Chen, X., Wang, Z., Zhang, X., Yu, Z., Wang, X., and Bian, D. (2018). A distributed cooperative control framework for synchronized reconnection of a multi-bus microgrid. *IEEE Transactions on Smart Grid*, 9(6):6646–6655.

[87] Shi, Y. and Eberhart, R. (1998). A modified particle swarm optimizer. In *1998 IEEE International Conference on Evolutionary Computation Proceedings. IEEE World Congress on Computational Intelligence (Cat. No.98TH8360)*, pages 69–73.

[88] Shi, Y. and Eberhart, R. C. (1998). Parameter selection in particle swarm optimization. In Porto, V. W., Saravanan, N., Waagen, D., and Eiben, A. E., editors, *Evolutionary Programming VII*, pages 591–600, Berlin, Heidelberg. Springer Berlin Heidelberg.

[89] Shi, Y. and Eberhart, R. C. (1999). Empirical study of particle swarm optimization. In *Proceedings of the 1999 Congress on Evolutionary Computation-CEC99 (Cat. No. 99TH8406)*, volume 3, pages 1945–1950 Vol. 3.

[90] Simpson-Porco, J. W., Shafiee, Q., Dörfler, F., Vasquez, J. C., Guerrero, J. M., and Bullo, F. (2015). Secondary frequency and voltage control of islanded microgrids via distributed averaging. *IEEE Transactions on Industrial Electronics*, 62(11):7025–7038.

[91] Sreekumar, P. and Khadkikar, V. (2016). A new virtual harmonic impedance scheme for harmonic power sharing in an islanded microgrid. In *2016 IEEE Power and Energy Society General Meeting (PESGM)*, pages 1–1.

[92] Taher, S. A. and Mansouri, S. (2014). Optimal pi controller design for active power in grid-connected sofc dg system. *International Journal of Electrical Power & Energy Systems*, 60:268 – 274.

[93] Tao Liu, Xiang Hao, Xu Yang, Ming Zhao, Qingyun Huang, and Lang Huang (2012). A novel repetitive control scheme for three-phase grid-connected inverter with lcl filter. In *Proceedings of The 7th International Power Electronics and Motion Control Conference*, volume 1, pages 335–339.

[94] Teodorescu, R., Blaabjerg, F., Liserre, M., and Loh, P. C. (2006). Proportional-resonant controllers and filters for grid-connected voltage-source converters. *IEE Proceedings - Electric Power Applications*, 153(5):750–762.

[95] Thomas Weise (2008). Global optimization algorithms - theory and application. *Online available at http://www.it-weise.de/*.

[96] Tsang, K. M. and Chan, W. L. (2005). Cascade controller for DC/DC buck convertor. *IEE Proceedings - Electric Power Applications*, 152(4):827–831.

[97] Wouters, C. (2015). Towards a regulatory framework for microgrids—the singapore experience. *Sustainable Cities and Society*, 15:22 – 32.

[98] Wu, D., Tang, F., Guerrero, J. M., Vasquez, J. C., Chen, G., and Sun, L. (2014). Autonomous active and reactive power distribution strategy in islanded microgrids. In *2014 IEEE Applied Power Electronics Conference and Exposition - APEC 2014*, pages 2126–2131.

[99] Yuhui Shi and Eberhart, R. C. (2001). Fuzzy adaptive particle swarm optimization. In *Proceedings of the 2001 Congress on Evolutionary Computation (IEEE Cat. No.01TH8546)*, volume 1, pages 101–106 vol. 1.

[100] Zhong, Q. and Hornik, T. (2013). Cascaded current–voltage control to improve the power quality for a grid-connected inverter with a local load. *IEEE Transactions on Industrial Electronics*, 60(4):1344–1355.

[101] Zhong, Q.-C. and Hornik, T. (2013). *Control of Power Inverters in Renewable Energy and Smart Grid Integration*. Wiley-IEEE Press, Englewood Cliffs (N.J.).

[102] Zhong, Q. C. and Zeng, Y. (2016). Universal droop control of inverters with different types of output impedance. *IEEE Access*, 4:702–712.

[103] Zhu, Y., Liu, B., Wang, F., Zhuo, F., and Zhao, Y. (2015). A virtual resistance based reactive power sharing strategy for networked microgrid. In *2015 9th International Conference on Power Electronics and ECCE Asia (ICPE-ECCE Asia)*, pages 1564–1572.

[104] Zhu, Y., Zhuo, F., and Shi, H. (2013). Accurate power sharing strategy for complex microgrid based on droop control method. In *2013 IEEE ECCE Asia Downunder*, pages 344–350.

[105] Ziouani, I., Boukhetala, D., Darcherif, A. M., Amghar, B., and Abbassi, I. E. (2017). A hierarchical control for flexible single-phase microgrid based on parallel vsis. pages 178–182.

[106] Ziouani, I., Boukhetala, D., Darcherif, A.-M., Amghar, B., and Abbassi, I. E. (2018a). Enhancing the power quality of an islanded microgrid including renewable energy sources. *International Conference on MATERIALS & ENERGY (ICOME18)*.

[107] Ziouani, I., Boukhetala, D., Darcherif, A.-M., Amghar, B., and Abbassi, I. E. (2018b). Hierarchical control for flexible microgrid based on three-phase voltage source inverters operated in parallel. *International Journal of Electrical Power & Energy Systems*, 95(C):188 – 201.